Bull Volcanol (2007) 69:581–608
DOI 10.1007/s00445-006-0096-z

RESEARCH ARTICLE

Magma evolution of Quaternary minor volcanic centres in southern Peru, Central Andes

Adélie Delacour · Marie-Christine Gerbe · Jean-Claude Thouret · Gerhard Wörner · Perrine Paquereau-Lebti

Received: 1 December 2005 / Accepted: 13 September 2006 / Published online: 17 November 2006

Abstract Minor centres in the Central Volcanic Zone (CVZ) of the Andes occur in different places and are essential indicators of magmatic processes leading to formation of composite volcano. The Andahua–Orcopampa and Huambo monogenetic fields are located in a unique tectonic setting, in and along the margins of a deep valley. This valley, oblique to the NW–SE-trend of the CVZ, is located between two composite volcanoes (Nevado Coropuna to the east and Nevado Sabancaya to the west). Structural analysis of these volcanic fields, based on SPOT satellite images, indicates four main groups of faults. These faults may have controlled magma ascent and the distribution of most centres in this deep valley shaped by en-echelon faulting. Morphometric criteria and ^{14}C age dating attest to four main periods of activity: Late Pleistocene, Early to Middle Holocene, Late Holocene and Historic. The two most interesting features of the cones are the wide compositional range of their lavas (52.1 to 68.1 wt.% SiO_2) and the unusual occurrence of mafic lavas (olivine-rich basaltic andesites and basaltic andesites). Occurrence of such minor volcanic centres and mafic magmas in the CVZ may provide clues about the magma source in southern Peru. Such information is otherwise difficult to obtain because lavas produced by composite volcanoes are affected by shallow processes that strongly mask source signatures. Major, trace, and rare earth elements, as well as Sr-, Nd-, Pb- and O-isotope data obtained on high-K calc-alkaline lavas of the Andahua–Orcopampa and Huambo volcanic province characterise their source and their evolution. These lavas display a range comparable to those of the CVZ composite volcanoes for radiogenic and stable isotopes ($^{87}Sr/^{86}Sr$: 0.70591–0.70694, $^{143}Nd/^{144}Nd$: 0.512317–0.512509, $^{206}Pb/^{204}Pb$: 18.30–18.63, $^{207}Pb/^{204}Pb$: 15.57–15.60, $^{208}Pb/^{204}Pb$: 38.49–38.64, and $\delta^{18}O$: 7.1–10.0‰ SMOW), attesting to involvement of a crustal component. Sediment is absent from the Peru–Chile trench, and hence cannot be the source of such enrichment. Partial melts of the lowermost part of the thick Andean continental crust with a granulitic garnet-bearing residue added to mantle-derived arc magmas in a high-pressure MASH [melting, assimilation, storage and homogenisation] zone may play a major role in magma genesis. This may also explain the chemical characteristics of the Andahua–Orcopampa and Huambo magmas. Fractional crystallisation processes are the main governors of magma evolution for the Andahua–Orcopampa and Huambo volcanic province. An open-system evolution is, however, required to explain some O-isotopes and some major and trace elements values. Modelling of AFC processes suggests the Charcani

Editorial responsibility: J. White

A. Delacour · M.-C. Gerbe
Département de Géologie–Pétrologie–Géochimie,
Université Jean Monnet and UMR 6524 Magmas et Volcans,
23 rue du Dr. Paul Michelon,
42 023 Saint-Étienne Cedex, France

J.-C. Thouret · P. Paquereau-Lebti
Laboratoire Magmas et Volcans, Université Blaise Pascal,
CNRS and OPGC,
5 rue Kessler,
63 038 Clermont-Ferrand Cedex, France

G. Wörner
Geowissenschaftliches Zentrum Göttingen, Abt. Geochemie,
Universität Göttingen,
Goldschmidtstrasse 1,
37 077 Göttingen, Germany

A. Delacour (✉)
Department of Earth Sciences, ETH Zurich,
Clausiusstrasse 25,
CH-8092 Zurich, Switzerland
e-mail: adelie.delacour@erdw.ethz.ch

gneisses and the local Andahua–Orcopampa and Huambo basement may be plausible contaminants.

Keywords Peruvian Andes · Monogenetic cones · Quaternary activity · Magma source · Deep crustal assimilation · Fractional crystallization

Introduction

The Andahua–Orcopampa and Huambo (AOH, 15°10′S–16°S, 72°30′W–72°W) volcanic province comprises three monogenetic fields located in the Central Volcanic Zone (CVZ) of the Andes in southern Peru (Fig. 1). Active volcanism in the CVZ is mainly characterised by formation of large composite volcanoes. They reach 2,000 to 3,000 m in structural height and have life times of generally about 0.8 to 0.6 M.y. and sometimes up to several M.y. These composite volcanoes consist of a variety of volcanic structures and edifices, with varying evolutionary styles (e.g. dome clusters, simple and compound cones dominated by pyroclastic deposits or lava flows, composite cones). Erupted magmas mainly belong to the high-K, calc-alkaline series and their compositions range from rare basaltic andesites to rare rhyolites, with large volumes of andesites and dacites. Some large centres have rather uniform compositions, whereas some others show large compositional ranges.

Minor volcanic centres, mainly monogenetic, are rare in southern Peru. There are minor shoshonitic centres in the vicinity of Cuzco, and scattered scoria cones near the Nevado Coropuna, north of the Nevado Solimana, and east of the Nevado Sara-Sara. The Andahua–Orcopampa and Huambo fields are characterised by an unusual abundance of such minor centres and associated lava flows. The Andahua–Orcopampa monogenetic field is located in and along the margins of a series of NNW–SSE trending en-echelon valleys: Orcopampa, Andahua and Ayo valleys (Figs. 1 and 2a). They are located between the Nevado Coropuna to the east and the Rio Colca to the west (Figs. 1 and 2a). The second monogenetic field is located close to Huambo, on the left side of the Rio Colca, in the Andean highlands close to the Nevado Sabancaya. It consists of a northern and a southern volcanic field (Fig. 2a). In the Orcopampa–Andahua valleys, more than 15 cones (Fig. 2a) are concentrated in an area of approximately 240 km^2 (about 40 by 6 km). They are associated with large lava flows, which cover more than 50% of the valley floor. Another young isolated monogenetic cone, Cerro Nicholson is found near Yura (Fig. 1) in the vicinity of the Huanca thrust fault. The Andahua–Orcopampa and Huambo volcanic province, as well as the Cerro Nicholson monogenetic scoria cone represent brief periods of volcanic activity. Their lavas display a rather wide compositional range, from unusually mafic olivine-rich basaltic andesites to dacites.

Although also found in other areas in the CVZ (e.g. El Negrillar Field near Socompa volcano in Northern Chile, Deruelle 1982; Antofalla field in Argentina, Allmendiger et

Fig. 2 **a** Location map of the volcanic province and the three monogenetic fileds on a SPOT satellite image (as of 1998). Volcanic cones and sample numbers are shown on this map, as well as the location of the Fig. 3**a**–**c** and Fig. 4**a**–**d**. **b** Structural map of the Andahua–Orcopampa and Huambo monogenetic fields showing the main four groups of faults identified

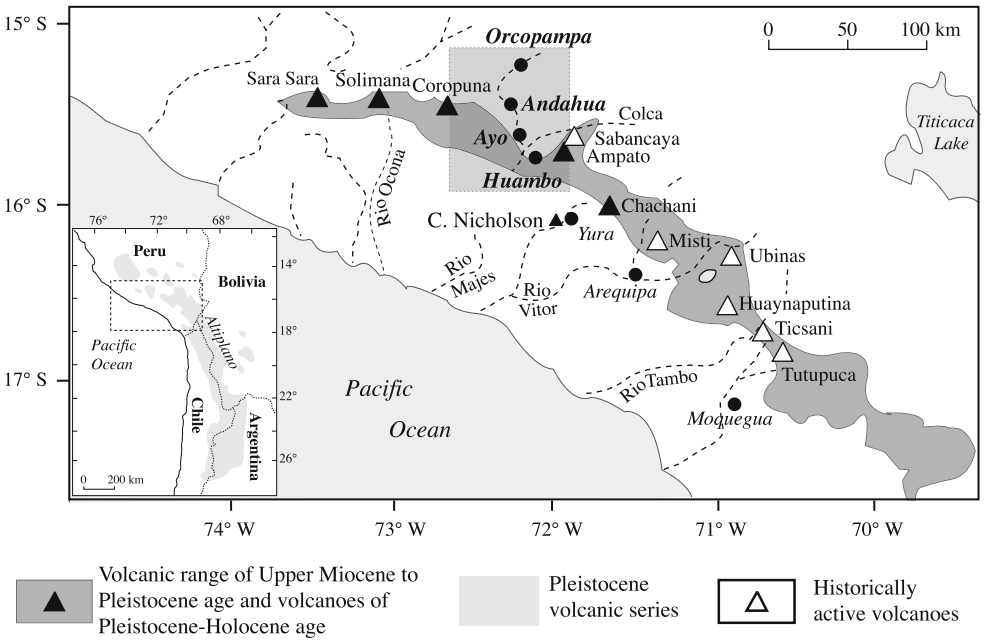

Fig. 1 Location map of the Central Volcanic Zone of southern Peru. The *grey box* shows the studied area, i.e. the Andahua–Orcopampa and Huambo volcanic province. Toward the ESE of this province, the minor volcanic Cerro Nicholson centre (a scoria and lava cone) showing similar characteristics to those of Andahua–Orcopampa and Huambo cones, is located near Yura. The place of the Andahua–Orcopampa and Huambo volcanic province in the Central Andes and the overall Andean Cordillera is shown in the *inset* map (*dashed-box*)

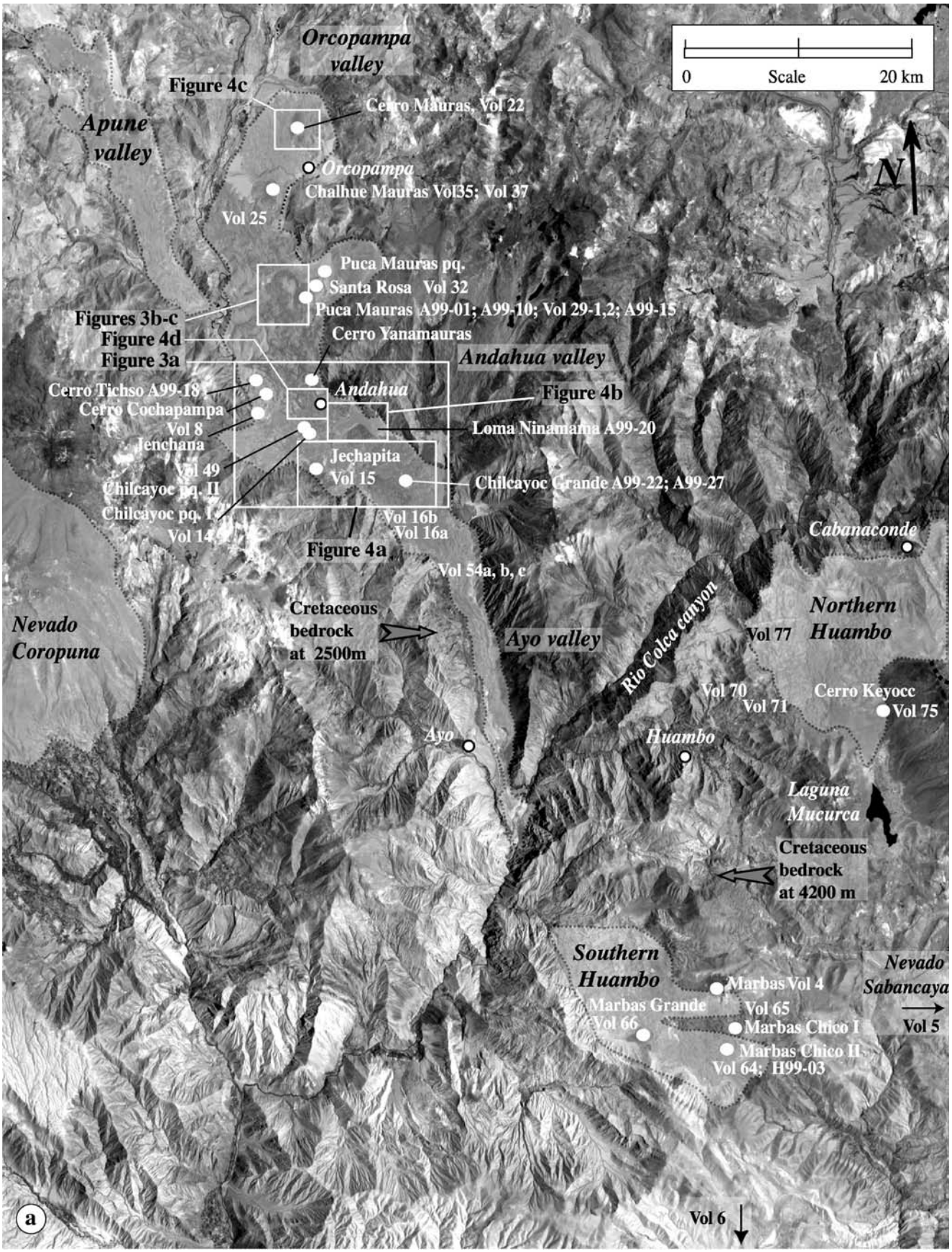
Orcopampa valley
Figure 4c
Cerro Mauras, Vol 22
Apune valley
Orcopampa
Chalhue Mauras Vol35; Vol 37
Vol 25
0 Scale 20 km
N
Puca Mauras pq.
Santa Rosa Vol 32
Puca Mauras A99-01; A99-10; Vol 29-1,2; A99-15
Figures 3b-c
Figure 4d
Figure 3a
Cerro Yanamauras
Andahua valley
Andahua
Figure 4b
Cerro Tichso A99-18
Cerro Cochapampa
Vol 8
Jenchana
Vol 49
Chilcayoc pq. II
Chilcayoc pq. I
Vol 14
Loma Ninamama A99-20
Jechapita
Vol 15
Chilcayoc Grande A99-22; A99-27
Vol 16b
Vol 16a
Figure 4a
Vol 54a, b, c
Cabanaconde
Nevado Coropuna
Cretaceous bedrock at 2500m
Ayo valley
Rio Colca canyon
Northern Huambo
Vol 77
Vol 70
Vol 71
Cerro Keyocc
Vol 75
Ayo
Huambo
Laguna Mucurca
Cretaceous bedrock at 4200 m
Southern Huambo
Marbas Vol 4
Marbas Grande
Vol 66
Vol 65
Marbas Chico I
Marbas Chico II
Vol 64; H99-03
Nevado Sabancaya
Vol 5
Vol 6
a

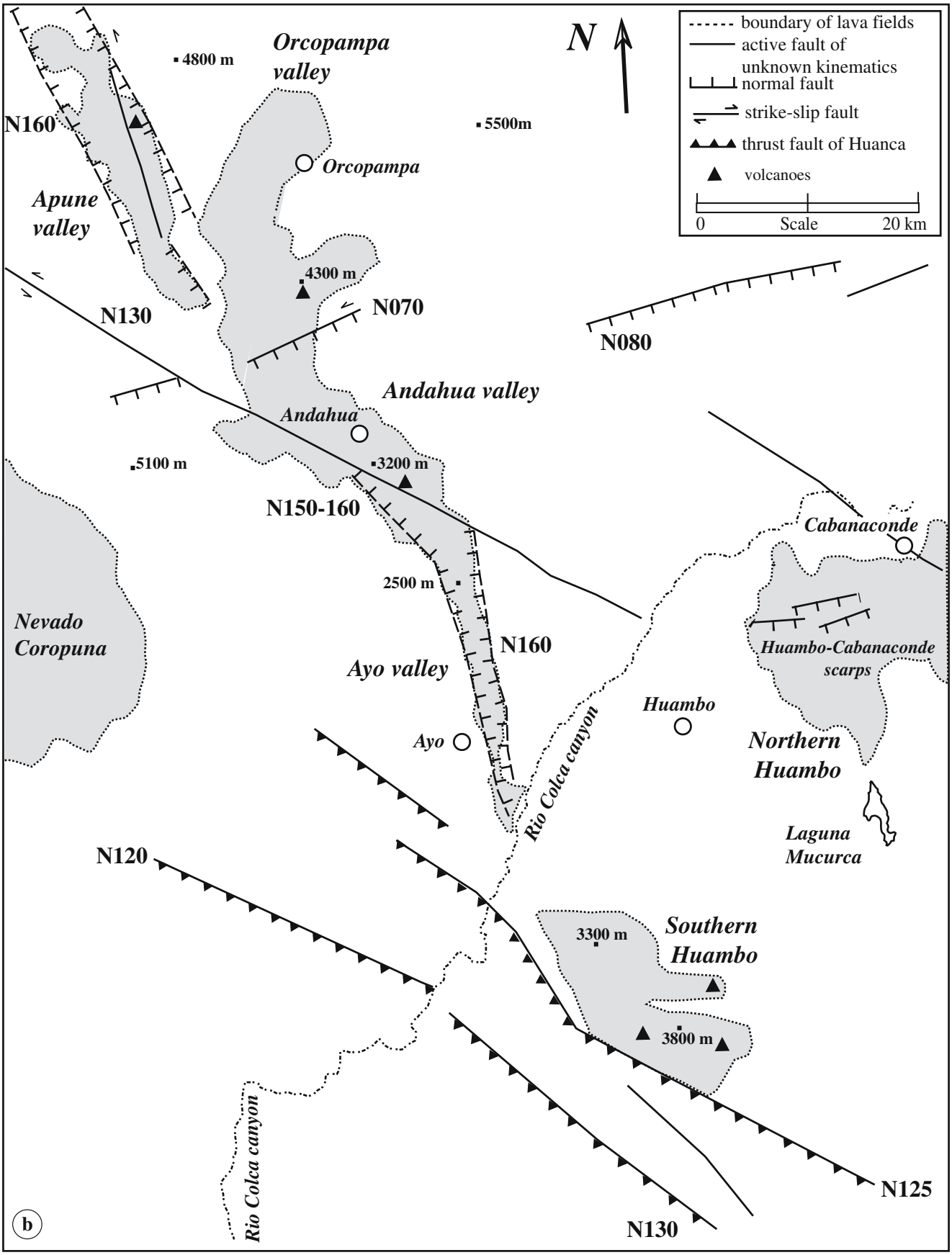
boundary of lava fields
active fault of unknown kinematics
normal fault
strike-slip fault
thrust fault of Huanca
volcanoes
0 Scale 20 km
N
Orcopampa valley
4800 m
5500m
N160
Orcopampa
Apune valley
4300 m
N130
N070
N080
Andahua valley
Andahua
5100 m
3200 m
N150-160
2500 m
Cabanaconde
Nevado Coropuna
N160
Huambo-Cabanaconde scarps
Ayo valley
Huambo
Ayo
Rio Colca canyon
Northern Huambo
Laguna Mucurca
N120
3300 m
Southern Huambo
3800 m
Rio Colca canyon
N125
N130
b

al. 1989; Kay et al. 1994), this type of volcanic activity during the Quaternary is quite unusual in the Andes. These monogenetic fields are virtually unstudied (Venturelli et al. 1978; De Silva and Xuming 2000) despite their unusual character. The contemporaneous and closely spaced occurrence of two distinct types of volcanism is an interesting feature that allows us to consider the influence of the size of magma reservoirs and the different modes of ascent and eruption on magma composition. The Andahua–Orcopampa and Huambo lavas, as well as Cerro Nicholson lavas, display petrographic and geochemical similarities to those of the composite volcanoes, as well as some differences from them. Our study will focus on the differences in order to highlight the nature of the parent magmas.

Current petrogenetic models for CVZ magmas call on extensive crustal contamination, but mechanisms and structural levels of this contamination remain in debate (James 1982; Barreiro and Clark 1984; Harmon and Hoefs 1984; Harmon et al. 1984; Thorpe et al. 1984; Hildreth and Moorbath 1988; Davidson et al. 1991; Aitcheson and Forrest 1994; Davidson and de Silva 1995). As the Peru–Chile trench is virtually sediment-free (Thornburg and Kulm 1987), the crustal component is not introduced to the source by melting of subducted sediments. Most importantly, modern CVZ magmas have systematically high Sm/Yb and Sr/Y ratios, which may reflect partial melting with garnet in the residues (Kay et al. 1987; Kay 2002). In the northern part of the CVZ, tectonic shortening resulted in significant thickening of the crust. This thickening induced an anomalous thermal regime in the lower crust that promotes partial melting of granulitic crustal material (Whitman et al. 1996; Kay et al. 1999). Such crust-derived melts may mix with mantle-derived magmas at deep levels, in a high-pressure MASH [melting, assimilation, storage and homogenisation] zone (Hildreth and Moorbath 1988; Kay 2002), producing large volumes of contaminated andesitic magmas. Low-pressure assimilation and fractional crystallisation (AFC) processes, magma mixing and crustal anatexis may also be involved at upper levels in the crust, in particular below large composite volcano complexes (James 1982; Barreiro and Clark 1984; Harmon and Hoefs 1984; Harmon et al. 1984; Thorpe et al. 1984; Hildreth and Moorbath 1988; Davidson et al. 1991; Aitcheson and Forrest 1994; Davidson and de Silva 1995). Petrological characteristics of the Andahua–Orcopampa and Huambo magmas suggest that they were erupted from deep reservoirs and have been less strongly modified in shallow magma chambers and feeder systems that appear to exist below many composite volcanoes. Thus, these Andahua–Orcopampa and Huambo lavas provide a window to the zone and processes where CVZ parent magmas may evolve.

SPOT (Satellite pour l'Observation de la Terre) satellite images, as well as field observations enable the identification of numerous fault structures in the Andahua–Orcopampa and Huambo volcanic province. A structural analysis has evaluated their potential activity during the Quaternary and has determined that a clear connection with the Andahua–Orcopampa and Huambo volcanic activity may be inferred, since tensional faulting prevails in the Western Cordillera of southern Peru (Sébrier and Soler 1991; Mering et al. 1996).

Geodynamic setting

The Central Andes (15–28°S) are part of an active continental margin mountain belt (Fig. 1), related to the convergence between the subducting oceanic Nazca plate and the South-American plate. The surface morphology above the 30° eastward-dipping downgoing slab (Barazangi and Isacks 1976; Cahill and Isacks 1992) is characterised from west to east by an active volcanic arc in the Western Cordillera, a broad high plateau (Altiplano in the north and Puna in the south) and an active eastward verging foreland belt. The present-day rate of convergence is 61±3 mm $year^{-1}$ at an azimuth of 79±4°, as estimated from space geodetic data at southern Peru latitude (Norabuena et al. 1998, 1999). Plate reconstructions suggest a peak convergence rate during Late Oligocene and a gradual deceleration of convergence since 20 Ma (Somoza 1998; Norabuena et al. 1999). This phase is also a period of major continental deformation that initiated the Andes' growth. The uplift of the thickened crust at the western edge of the continental block is an isostatic response to crustal shortening (James 1971; Isacks 1988; Zandt et al. 1994; Beck et al. 1996; Gregory-Wodzicki 2000; Beck and Zandt 2002). Geophysical data acquired in the past two decades have confirmed the extreme crustal thickening of the Central Andes. They also clarified the picture of the crustal structure in the Central Andes and demonstrated the variable nature of the mantle root (Whitman et al. 1992, 1996; Giese et al. 1999; Beck and Zandt 2002; Gerbault et al. 2005).

The Andahua–Orcopampa and Huambo volcanic province is located in the Western Cordillera, which supports the active magmatic arc. This magmatic arc, made up of andesitic to dacitic composite volcanoes, is placed about 120–130 km above the Wadati–Benioff plane and built on 60–80 km thick crust (Barazangi and Isacks 1976; Cahill and Isacks 1992; Beck and Zandt 2002). In the Western Cordillera and the Altiplano, a deep crustal root is evident from both gravimetric and seismic studies. Beneath the active volcanic arc, geophysical properties suggest partial removal of the mantle lithosphere, so that hot asthenospheric material is mainly filling the gap between the crust and the subducting plate (Whitman et al. 1992, 1996; Beck and Zandt 2002). Giese et al. (1999) address the question of

the petrological interpretation of these geophysical data. They suggest that the Moho discontinuity may not correspond to a boundary between crustal and mantle rocks. Hydration and metasomatism of peridotitic mantle rocks may change their petro-physical properties to typical crustal values. Furthermore, some authors propose that a thin lithospheric mantle lid is present beneath the crust of the Western Cordillera (Baumont et al. 2001).

The 60–80 km thick crust supporting the active volcanic arc has mainly a felsic to intermediate bulk composition (Beck and Zandt 2002). From thermo-mechanical properties, the shallow crust, up to 50 km deep, is predominantly felsic, whereas the lower crust tends to be mainly mafic (Yuan et al. 2002). A mid-crustal seismic low-velocity zone and high surface heat-flow argue for high-temperature conditions within the crust and widespread intra-crustal melting since Miocene and Pliocene times (Babeyko et al. 2002; Yuan et al. 2002). Numerical modelling of the thermo-mechanical properties of the crust suggests that convective heat and mass transfer from partially molten lower crust to shallower levels may result in high intra-crustal temperatures (Babeyko et al. 2002). Warm asthenospheric material possibly enhances heating and partial melting of the lower crust (Whitman et al. 1992, 1996; Babeyko et al. 2002). The mechanical decoupling is enhanced by a competent upper crust and a westward moving, ductile, middle to lower crust as shown by numerical models (Isacks 1988; Gerbault et al. 2005; Tassara 2005). The regional stress regime in the Central Andes causes horizontal ductile flow in the lower crust, which induces brittle deformation in the upper crust and small amounts of surface deformation with vertical uplift (Wörner et al. 2002; Victor et al. 2004; Gerbault et al. 2005). Indeed, the cold and rigid forearc acts as a mechanical barrier, resisting the relative motion of the ductile crustal material. This has caused crustal material, in response to tectonic shortening, to accumulate below the competent upper crust of the Western Cordillera (Babeyko et al. 2002). Observed active regional scale strike-slip faults, such as the N135-striking Ichupampa and Huanca faults in southern Peru (Mering et al. 1996; Antayhua et al. 2001), also indicate mass transfer in a direction roughly perpendicular to the direction of convergence. These structures only accommodate small amounts of displacement, suggesting that they are related to crustal block rotations responding to regional bending (Lamb 2000).

Analytical methods

Petrographic observations of thin sections of lavas (olivine-rich basaltic andesites, basaltic andesites, andesites and dacites) collected from the Andahua–Orcopampa and Huambo monogenetic fields were used to document the textural relationships and to identify mineral phases. Quantitative mineral chemistries have been determined with an electron microprobe CAMECA SX100 at the "Laboratoire Magmas et Volcans" of the Université Blaise Pascal in Clermont-Ferrand, France. Operating conditions for mineral analyses were 15 kV accelerating voltage, 15 nA beam current, 10 s counting times for major elements and 15 s for minor elements (Cr, Ni) and a focussed beam.

Major elements analyses and trace elements of whole-rock samples were performed by inductively coupled plasma-mass spectrometry (ICP-MS) and X-ray fluorescence (XRF) at three different laboratories. A first set of samples was analysed at Ecole Nationale des Mines of Saint-Etienne, France, by XRF method. Major elements and trace elements have been measured on glass pills and on compacted powder pills, respectively, with an analytical precision (2σ) less than 1% for major elements and around 5% for trace elements, except for Ni, Co, Cr and V, which have an analytical precision less than 10%. A second set of samples was analysed at CRPG-Nancy, France, by ICP-AES and ICP-MS after fusion with $LiBO_2$ and dissolution by HNO_3. The analytical precision (2σ) is less than 1% for major elements (except for Ca, Na and Ti: 2% and Mn: 5%), and less than 10–15% for trace elements (if concentrations are higher than 50 ppm, the analytical precision is less than 5–10%). The REE of these two sets of samples have been separated and concentrated by ion-exchange chromatography, and analysed by ICP-AES at Ecole Nationale des Mines of Saint-Etienne, with an analytical precision (2σ) estimated to be less than 10% from systematic in-run analysis of international standard BCR2 (basalt from USGS). In addition, a third set of whole-rock analyses (major and trace elements, and REE) were performed at Geowissenschaftlisches Zentrum of Göttingen Georg-August Universität, Abteilung Geochemie, Germany. Major elements and some trace elements (Sc, V, Cr, Co, Ni, Zn, Ga, Rb, Sr, Zr, and Ba) were determined by X-ray fluorescence (XRF) analysis on glass pills prepared with a lithium tetraborate flux. The analytical precision (2σ) is less than 1% for major elements (except for Fe, Na: 2% and LOI: ~10%) and around 5% for trace elements. Additional trace elements were analysed by ICP-MS. The analytical errors estimated according to rock standards JB3 and JA2 are about 15–20% for Nb and Ta, and <10% for other trace elements. Cross-check analyses were performed to guarantee analytical consistency and the concordance between labs was found to be good; the combined data set is used for this study.

Sr-, Nd-, and Pb-isotope compositions have been measured on selected samples. Whole-rock powders were dissolved using an $HF/HNO_3/HClO_4$ mixture, and Sr and Nd elements were separated at the Department of Geology of the Université Jean Monnet in Saint-Etienne, France,

with ion-exchange chromatography according to the procedures described by Pin et al. (1994), and Pin and Santos Zalduegui (1997). $^{87}Sr/^{86}Sr$ and $^{143}Nd/^{144}Nd$ isotopic ratios were determined using a VG Isomass 54E multicollector mass spectrometer at the "Laboratoire Magmas et Volcans" (CNRS, Université Blaise Pascal, Clermont-Ferrand, France). During the period of measurements, SRM-987 and AMES Rennes standards gave $^{87}Sr/^{86}Sr=0.71026\pm0.00003$ (2σ, $n=7$) and $^{143}Nd/^{144}Nd=0.511960\pm0.000015$ (2σ, $n=4$), respectively. Sr-, Nd- and Pb-isotope compositions were also measured at Geowissenschaftlisches Zentrum of Göttingen Georg-August Universität, Abteilung Geochemie, Germany, with a Finnigan MAT 262 RPQII+ mass-spectrometer. During the period of analyses, standards NBS987 (0.710245) for Sr and LaJolla (0.511847) for Nd and NBS981 (recommended values from Todt et al. 1984) for Pb were measured. Statistical errors (2σ) were estimated less than 0.004% for Sr and Nd and less than 0.1% for Pb. For more details see Churikova et al. (2001).

Oxygen isotope ratios of whole-rock samples and mineral separates were determined after degassing under vacuum on a conventional line for 3 h at 250°C. The powders were reacted with BrF_5 at 550°C for 8 h and the extracted O_2 converted to CO_2 using a hot platinised carbon rod (Clayton and Mayeda 1963). Duplicate splits of the internal quartz standard (Murchinson Line Quartz, MQ) provided by the University of Cape Town were run with each batch of six samples. The $\delta^{18}O$ value of MQ has been accurately determined to be 10.1‰ VSMOW (Vennemann and Smith 1990) after calibration against the NBS-28 quartz international standard, assuming a value for NBS-28 of 9.64‰ VSMOW (Coplen 1993). Oxygen isotopic ratios were determined with a VG-prism mass spectrometer at the Ecole Normale Supérieure of Lyon (S.M.F. Sheppard). All data are reported in the familiar δ notation where $\delta^{18}O=(R_{sample}/R_{standard}-1)\times10^3$ and $R=^{18}O/^{16}O$. The average value obtained for MQ was used to normalise the $\delta^{18}O$ values on the SMOW scale. The average difference of 16 MQ duplicates analysed during the course of this work was less than 0.3‰. Thus 2σ-analytical precision of 0.3‰ for the O-isotope data is estimated and is mainly due to the extraction procedure, as the mass-spectrometer analytical precision is less than 0.010‰.

Accelerator mass spectrometry (AMS) ^{14}C age-dating was performed at the Isotope Research Center of Gröningen (Netherlands).

Volcanism and crustal structure in the Andahua–Orcopampa and Huambo volcanic province

The present day stress regime in southern Peru is controlled by: (1) north–south stretching, related to the extensional regime of the high Andean Cordillera and to the slow motion of the convergent plates, and; (2) east–west compression associated with the N80-trending convergent oceanic Nazca plate (Sébrier and Soler 1991; Mercier et al. 1992). Moreover, data obtained with SPOT and SAR ERS-1 satellite images (Mering et al. 1996) indicate that the tectonic regime in southern Peru close to Arequipa (Fig. 1) is controlled by two main faults: the NW-trending Huanca and Ichupampa faults. The extension in this area is NE–SW and the Huanca and Ichupampa faults form a discrete pull-apart structure in the vicinity of Arequipa that contains the Nevado Sabancaya volcano. These extensive zones along N70- and N135-trending faults are associated with fissures that allow the ascent of the magmas to the surface (Huaman et al. 1993).

The Andahua–Orcopampa and Huambo monogenetic fields extend roughly oblique to the NW–SE-trending volcanic range of the CVZ. The Andahua–Orcopampa monogenetic field lies in a NS-trending valley (Fig. 2a, b), divided into four segments, the N–S Orcopampa area, a NW–SE trending tributary valley to the west, WNW–ESE trending Andahua area and the N–S-trending Andahua–Ayo valley to the south. To the south of the Rio Colca Valley, the Huambo monogenetic field (Fig. 2a, b) displays a northern and a southern field. Within these two fields, the volcanic centres are roughly WNW–ESE-trending, parallel to the N120-trending Huanca thrust fault zone in the Western Cordillera (Mering et al. 1996; Antayhua et al. 2001). Lava flows are channelled towards the Pacific piedmont as far as 35 km from the Huanca fault scarp in southern field of Huambo.

A structural analysis of this part of the Western Cordillera suggests that the emplacement of the Andahua–Orcopampa and Huambo volcanic province is related to the regional stress regime and regional tectonic trends (Figs. 2a, b and 3a, b). The study of a 1998-SPOT satellite image shows four groups of faults in the Andahua–Orcopampa and Huambo areas (Fig. 2b). (1) N120 to N130-trending left-lateral strike-slip faults, e.g. in the Andahua area, are "en-echelon" faults. They accommodate the Orcopampa valley, to the north, and the Ayo valley, to the south (Figs. 2b and 3a). The left-lateral component is consistent with the present N80-trending convergence of the Nazca plate with the south-American plate. (2) Extensional N070–N080-trending faults have offset lava flows of late Pleistocene age (e.g., the two Huambo–Cabanaconde scarps, Fig. 2b), and the Holocene Puca Mauras lava field (Fig. 3b, c), and N80-trending extensional faults observed on satellite images have been analysed by Huaman et al. (1993) and Mering et al. (1996). (3) N130-trending thrust faults, with a southwest dip, affected the southern Huambo area (Fig. 2b). These regional thrusts, parallel to the Peru fore-arc trench, are inherited features from earlier stages in

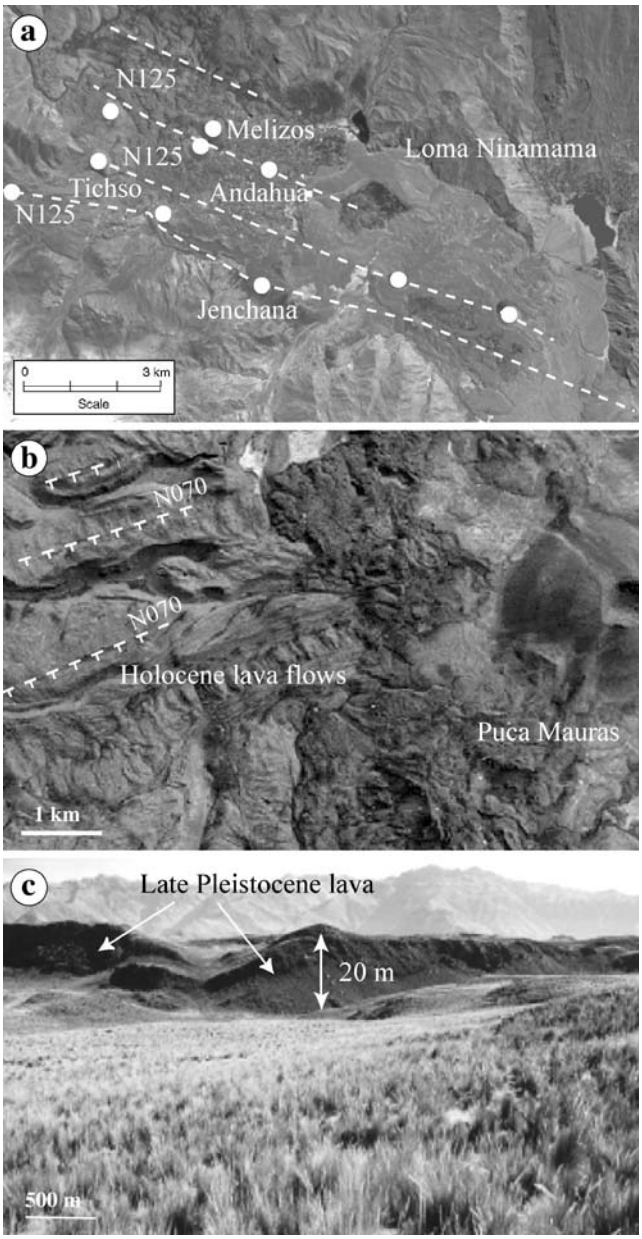

Fig. 3 **a** Valley of Andahua as shown by extracted scene of SPOT4 satellite (1998). White dots represent volcanoes and lava vents. Note that the monogenetic centres are aligned along N125–130 lineaments. **b** Aerial photograph of the lava terraces of the Puca Mauras volcano, showing that the N070-trending normal faults offset the Holocene lava flows. **c** Scarps showing the N070-trending normal faults in the Pleistocene lava flow

the formation of the Andes (Vicente et al. 1979). From one eruptive fissure, parallel to the N130-trending thrust fault, a recent lava flow has mantled the fault scarp west of Marbas Grande cone. (4) N010–N040-trending faults are inherited faults, which are often offset by active faults, e.g. in the Ayo area.

The north–south extensional regime in southern Peru may have reactivated the fault system identified within the Andahua–Orcopampa and Huambo province, especially the N120–N130-trending and N80-trending faults. These faults may be deeply penetrative and may provide pathways for magma ascent from deep reservoirs (Huaman et al. 1993; Mering et al. 1996). The Andahua–Orcopampa and Huambo volcanic centres may thus be representative of parental magmas feeding the composite volcanoes.

Morphology, volume, and age of the Andahua–Orcopampa and Huambo cones and lava flows

Morphology of the cones

Monogenetic scoria and cinder cones of moderate size (200–300 m high and 500–650 m across) are the predominant volcano type in the Andahua–Orcopampa and Huambo monogenetic fields, and were each formed during a single eruption. About 60 cones are found in the Andahua–Orcopampa and Huambo volcanic province, with 40 of them concentrated between Orcopampa and Ayo (Fig. 2a). Most of the cones lie on the valley floors (e.g. Chilcayoc Grande or Jechapita, Fig. 4a) but a few edifices have been built on the Miocene to upper Cretaceous rocks of the valley sides. For instance, Cerro Jenchaña (Fig. 3a) is built on Cretaceous sandstone forming the western scarp of the Andahua valley and Cerro Ticshó has grown on Pleistocene lava bedrock of the Orcopampa group (Caldas 1993). Lavas of these scoria cones often contain sedimentary xenoliths and xenocrysts, suggesting partial digestion of bedrock fragments in magmas. Some lava flows associated with the cones extend as far as 4 to 8 km (e.g. Loma Ninamama; Fig. 4b), and extensive compound block-lava flows have a total estimated volume of 15± 5 km^3. Thick lava fields cover the floors of the Orcopampa–Andahua valleys to thicknesses of up to 130 m in the Ayo valley. Thinner lava flows, a few tens of meters thick, cover parts of the northern and southeastern Huambo fields.

Ages

A number of methods were used to estimate the chronology of the volcanic activity in the Andahua–Orcompampa and Huambo volcanic province: (1) ^{14}C age dating, (2) morphometric classification of the edifices, and (3) relative dating using stratigraphical relationships, surface morphology criteria and the degree of weathering on surfaces, based on interpretation of aerial photographs and field observations. Previous K–Ar dating of the andesitic bedrocks near Andahua indicated Middle to Late Pleistocene ages (Kaneoka and Guevara 1984). One sample collected north of the Cerro Tichsó (WNW of the town of Andahua)

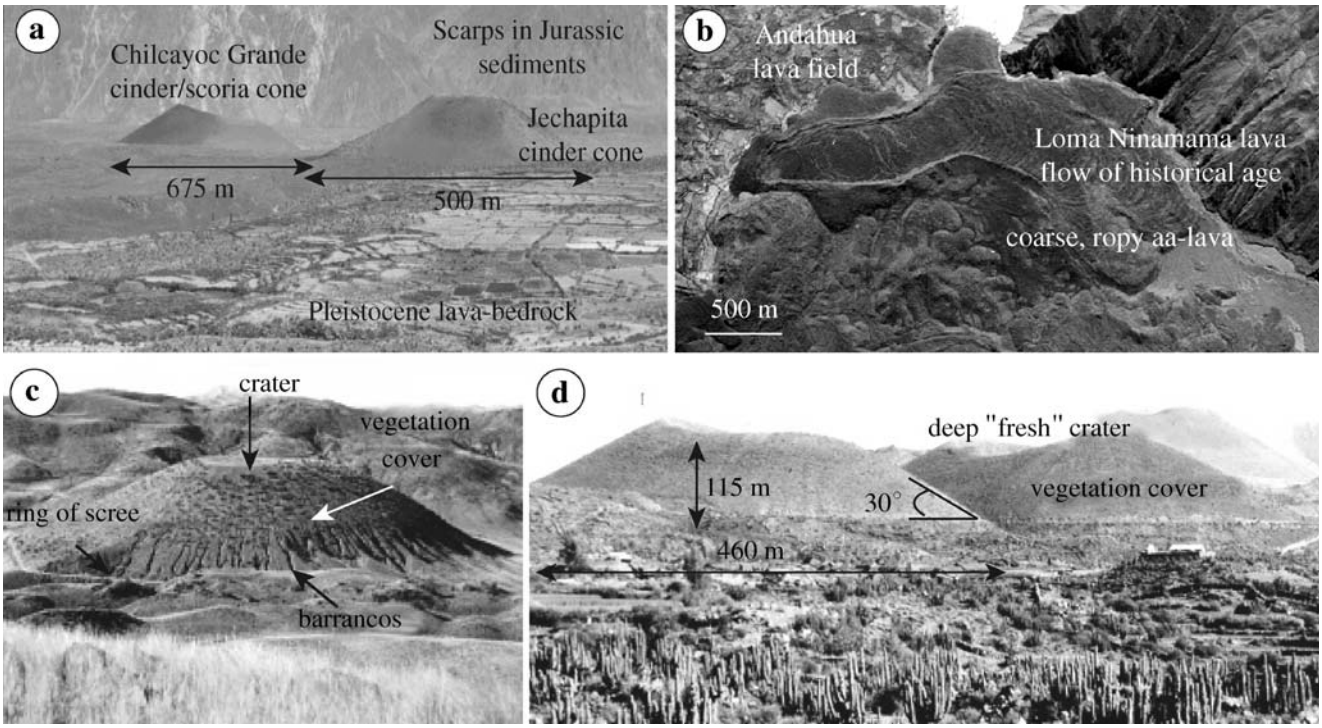

Fig. 4 **a** Photograph of the Jechapita and Chilcayoc Grande cones that are typically well preserved cinder and scoria cones in the Andahua field. These cones are built on Middle Pleistocene age lava bedrock. **b** Aerial photograph of the historical Loma Ninamama coarse ropy lava flow, east of Andahua village. **c** Marbas Chico cone of middle Holocene age (southern Huambo area), showing surface-modifications, e.g. gullies, subdued crater, and vegetation cover. **d** "fresh" Mellizos cinder and scoria cones (Andahua village), showing no trace of degradation, no deep craters and no vegetation cover. The morphometric values (*D*, *S*, and *H*) of one cone are shown on this photograph (see text for discussion and Fig. 5)

yielded an age of 0.27±0.02 Ma, and a second one sampled south of the Yanamauras cones provided an age of 0.5± 0.07 Ma (Table 1).

Four ^{14}C ages point to limited eruptive activity during Middle and Late Holocene times. The ages and locations of the analysed samples are presented in Table 1. Some monogenetic cones may even have been active in historical times, particularly in the Andahua field, as suggested by one of the ashfall layers of Jenchaña cinder cone, which is directly overlain by the A.D. 1600 Huaynaputina ash deposit (Thouret et al. 2002). The two ashfall layers are in sharp and regular contact without intercalated soil, implying a short time interval between the two events. Age determinations thus range from Late Pleistocene to possibly historic eruptions. The older ages overlap with those of similar mafic centres north of Coropuna and in the Colca Canyon to the NE of the Andahua–Orcopampa and Huambo monogenetic fields. Voluminous Holocene eruptions of minor centres, however, are clearly restricted to the three fields studied here.

The denudation rates of the Andahua–Orcopampa and Huambo edifices have been estimated from measurements on topographic maps (scale: 1/25,000) and aerial photographs in order to determine the relative age of the volcanic cones (Appendix A). The four morphometric parameters utilized (following Wood 1980) are: (1) the basal diameter

Table 1 Ages of edifices and lava flows of the Andahua–Orcopampa and Huambo volcanic fields (A: Andahua, O: Orcopampa, H: Huambo)

Location	Volcanic fields	Methods	Material dated and deposit	Age
Cerro Tichsó	A	^{14}C[a]	Burned twigs in ash	4,060±50 year BP
Cerro Mauras I	A–O	^{14}C[a]	Organic matter from a peat in ash	2,810–2,970±50 year BP
Cerro Keyocc	H	^{14}C[a]	Peat in ash	2,650±50 year BP
Chilcayoc Grande	A	^{14}C[a]	Charcoal in ash	1451 to 1523 A.D.
Lava-bedrock north of Cerro Tichsó	A–O	K/Ar[b]	Whole-rock	0.27±0.02 Ma
Lava-bedrock south of Andahua	A	K/Ar[b]	Whole–rock	0.5±0.07 Ma

[a] Conventional analyses made at the Isotope Research Centre of Gröningen (Netherlands)
[b] Kaneoka and Guevara (1984)

D_b, (2) the crater diameter D_{cr}, (3) the edifice height H, and (4) the slope average dip S, with $S=\tan^{-1}(H/(D_b-D_{cr}))$. A decrease in the ratio of height (H) to basal diameter (D_b) is the consequence of height reduction due to erosion and to the fact that the basal diameter increases as scree accumulates. From the measured H/D_b ratios, the Andahua–Orcopampa and Huambo edifices may be classified into two relative age groups (Fig. 5a) according to erosion stages, as described by Wood (1980): (1) The "Andahua age" applies to cones less than 5,000 years old with H/D_b ratios in the range 0.25–0.35, and (2) the "Orcopampa age" applies to cones 6,000 to 20,000 years old with moderate denudation rate and H/D_b ratios of 0.1–0.25. Based on the measured morphometric parameters, the average slope angle of cone flanks (Fig. 5b) decreases with H/D_b ratio and hence with age. Therefore a slope range for each edifice generation can be used as a criterion for relative chronology: (a) 30 to 35° for late Holocene and historical Andahua cones; (b) 20 to 28° for the Early to Middle Holocene Orcopampa cones; and (c) 15 to 20° for the oldest Orcopampa cone group of Late Pleistocene age (Fig. 5a).

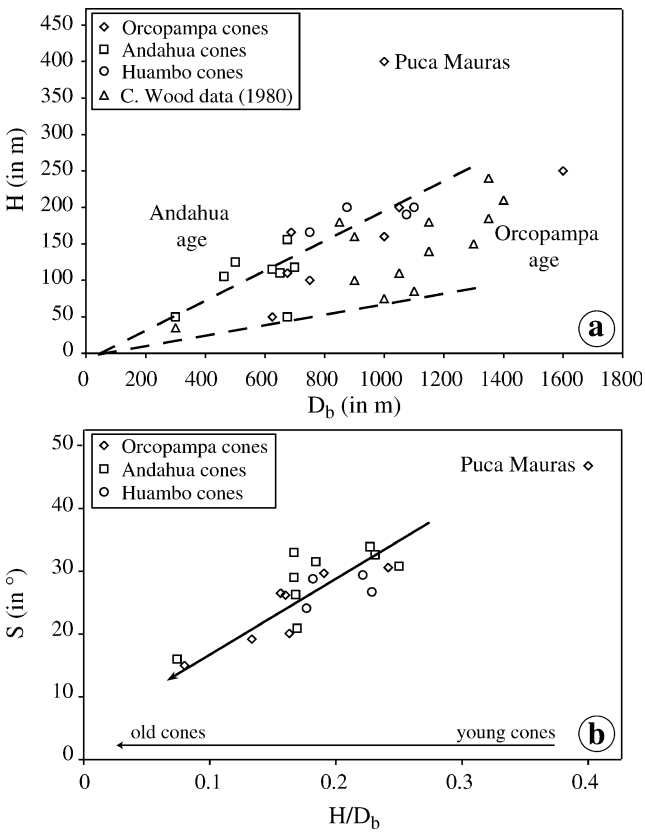

Fig. 5 Graphs showing morphometric statistical data. **a** H versus D_b diagram, defining two age groups: the Andahua cones for the historical and late Holocene edifices and the Orcopampa cones for the Early to Middle Holocene and late Pleistocene edifices. Puca Mauras showing different features is out of the two trends. **b** S versus H/D_b diagram, showing the linear evolution of cone slopes with H/D_b ratio

The stratigraphical relationships, surface morphology (e.g. drainage density, vegetation cover, crater shape; Colton 1967) and weathering stages indicate the same four periods of volcanic activity: Late Pleistocene, Early to Middle Holocene, Late Holocene and historical time. For instance, some cones, e.g. Marbas Chico I (southern Huambo field, Fig. 2a) and Cerro Mauras II (Orcopampa field, Fig. 2a), display characteristics of at least Early to Middle Holocene age (e.g. subdued crater, deep barrancos, vegetation cover; Fig. 4c), whereas the fresh morphology of the Andahua cones (deep craters, steep slopes without gullies, no soil and scattered vegetation, e.g., Mellizos volcanoes, Fig. 4d) indicates Late Holocene eruptive activity.

Petrography and mineralogy of the Andahua–Orcopampa and Huambo lavas

Textures as well as mineral assemblages are similar throughout the Andahua–Orcopampa and Huambo monogenetic fields irrespective of age, size and morphology of the eruptive centres (Table 2). The Andahua–Orcopampa and Huambo minor centres, and Cerro Nicholson lavas and tephra are generally dark, subaphyric to poorly porphyritic, and variably vesicular (0–70 vol.%). The lavas often exhibit trachytic textures. Fewer than 10% of the lavas are porphyritic; these contain up to 15 vol.% phenocrysts, which are generally 200–600 μm and rarely up to 1 mm in size.

Plagioclase is the prominent mineral phase, except in a few rare cases (e.g. vol6 and vol58) in which olivine and clinopyroxene occur in equal proportions with plagioclase. Clinopyroxene and Fe–Ti oxides are present in all petrographic types. Olivine is found in olivine-rich basaltic andesites and is also present, though rare, in some andesites. Hornblende and orthopyroxene also appear in the andesites, whereas biotite phenocrysts are found only in the most evolved dacite (A99-08).

Matrix textures are generally microlitic (crystal size less than 80 μm) and more rarely microcrystalline (crystal size of 80–200 μm), with brownish interstitial glass. These textural features are quite different from those of eruptive products from the large composite stratovolcanoes. Their lavas, generally more porphyritic, contain up to 25 vol.% phenocrysts with sizes frequently exceeding 1–2 mm (e.g. Nevado Sabancaya recent lavas, Gerbe and Thouret 2004).

The compositional ranges for minerals in the four distinct petrographic types (olivine-rich basaltic andesites, basaltic andesites, andesites and dacites) are summarized in Table 3.

Plagioclase composition shows decreasing anorthite contents from olivine-rich basaltic andesites to dacites.

Table 2 Textural and mineralogical characteristics of lavas from the Andahua–Orcopampa and Huambo volcanic fields and from the Cerro Nicholson cone

Volcanic fields	Orcopampa field	Andahua field	Huambo field	Cerro Nicholson
Lavas and cones				
Texture	Microlitic	Microlitic	Microlitic to porphyritic	Porphyritic
Vesicularity (%)	10–70	10–70	10–70	0–70
Compositional range	Basaltic andesites to dacites	Basaltic andesites to andesites	Olivine-rich basaltic andesites to andesites	Olivine-rich basaltic andesites
Mineral assemblage				
Basalts			pl+cpx+ol+mt	pl+cpx+ol
Basaltic andesites	pl+cpx+ol+mt	pl+ol+cpx+mt	pl+cpx+ol+mt	
Andesites	pl+px+ol±hb+mt	pl+cpx±ol±hb+mt	pl+px±ol±hb+mt	
Dacites	pl±cpx±hb±biot+mt			
Pleistocene lavas of the bedrock				
Texture		Porphyritic	Porphyritic	
Vesicularity (%)		0–20	10–15	
Compositional range		Andesites	Andesites	
Mineral assemblage		pl+px±ol		

The mineral assemblages of each petrographic type are reported (*pl* plagioclase, *ol* olivine, *px* orthopyroxene and clinopyroxene, *hb* hornblende, *biot* biotite, *mt* Fe–Ti oxides).

Most phenocrysts and microphenocrysts display normal optical and compositional zoning, with a decrease of ca. 5–15% An from core to rim. Nevertheless, plagioclases in some andesites (vol16b, vol70) show reverse stepped-zoning with low-amplitude oscillatory zoned cores, usually bounded by sharp resorption surfaces and mantled by 50-μm thick inclusion-rich rims with higher An contents. Large An-contrasts (>10%) associated with resorption may be caused by injection of more mafic magmas into differentiated magmas in reservoirs feeding the volcano (Gerbe and Thouret 2004; Ruprecht et al. 2006).

Euhedral olivine phenocrysts and microphenocrysts form about 25% of the crystal content (i.e. ca. 5 vol.% of the rock) in the olivine-rich basaltic andesites (vol6, vol58). In

Table 3 Types and compositional range of minerals in the four distinct petrographic types of the Andahua–Orcopampa and Huambo monogenetic fields and the Cerro Nicholson cone

Petographic types (sample nb)		Olivine-rich basaltic andesite 3	Basaltic andesites 13	Andesites 51	Dacites 2	Comments
Plagioclase	% An pheno.	63–72	53–71	34–60	29–38	Mainly normal zoning with an amplitude of 5–15% An and rarely oscillatory zoning
	% An μpheno.	63–67	55–64	35–54	33–49	
Clinopyrox.	% Wo	31–49	31–43	31–43		
	Composition range	Calcic augite and diopside	Calcic augite	Calcic augite		
Orthopyrox.	% En			67–75		
Olivine	% Fo	80–86	74–83	71–79		Basalt olivines contain Cr–spinel inclusions
	Ni (ppm)	470–2,120	175–390	500–1,250		
	Cr (ppm)	135–890	136–410	130–810		
Amphibole				Magnesio-hastingsite-Tschermakite		Amphibole show reaction rims of Fe–Ti oxides (ilmenite and magnetite)
Biotite					$1.14<Al^{T}<1.28$	
Fe–Ti oxides		<-Ulvöspinel–magnetite and ilmenite series->				

Number of samples from each petrographic type is based on samples analysed for whole-rock chemistry (major and trace elements).

andesites, olivine crystals are very rare, and often display anhedral resorbed shapes suggesting that they may be xenocrysts. Concomitant to modal variations, olivines decrease from Fo_{85} to Fo_{70} (Table 3) with increasing degree of magmatic differentiation. In olivine-rich basaltic andesites, olivine displays an average composition of Fo_{85} and contains chromian spinel inclusions, which show a limited range of Mg-numbers and Cr-numbers (40–55 and 50–65, respectively). These homogeneous compositions are consistent with equilibrium crystallisation with Fo_{85}-olivine at high temperature (Irvine 1967; Fisk and Bence 1980; Dick and Bullen 1984). These authors have also demonstrated that coexisting Cr-spinel and olivine are highly sensitive to subsolidus exchange of Mg and Fe, due to changes in intensive parameters like temperature and oxygen fugacity. This narrow range of Cr-spinel composition may suggest that magmas did not suffer long storage prior to eruption. Nevertheless, compositions of both Cr-spinel and coexisting olivine suggest that they formed in magmas that had already suffered some differentiation compared to primary mantle melts.

Clinopyroxene is ubiquitous in all lavas and has a diopside–calcic augite composition (Table 3; Morimoto 1988). Clinopyroxene composition is overall more calcic in the olivine-rich basaltic andesites where diopside is found as phenocrysts, whereas Mg- and Ca-rich augite exhibits very homogenous compositions in all other petrographic types. Orthopyroxene in andesites exhibits a narrow compositional range from En_{67} to En_{75} (Table 3). Amphiboles rarely occur in andesites and dacites (Table 3), and plot within the field of magnesio-hastingsite or, rarely, in the tschermakite field (Leake et al. 1997), with Al_2O_3 and TiO_2 contents spanning ranges of 10–13 wt.% and 3 to 4 wt.%, respectively.

The mineralogy of the Andahua–Orcopampa and Huambo lavas is thus characteristic of calc–alkaline lavas of the Central Andean Volcanic Zone, with plagioclase, pyroxene and amphibole crystals showing a typical calcic compositional range. The unusual feature of the Andahua–Orcopampa and Huambo lavas is the occurrence of olivines with high-forsterite contents and chromian spinels as inclusions in the olivine-rich basaltic andesites.

Pre-eruptive temperatures have been estimated for the basaltic andesites using the distribution of Fe^{2+} and Mg^{2+} between olivine and liquid (Roeder and Emslie 1970; Leeman 1978) and from the distribution of CaO/MgO between olivine and liquid (Jurewicz and Watson 1988). In andesites and dacites, temperature estimates were obtained with the Fe–Ti oxide geothermometer, using the calculation scheme of Spencer and Lindsley (1981) for pairs of magnetite and ilmenite that satisfied the equilibrium Mg–Mn partitioning test (Bacon and Hirschmann 1988). In cases where clinopyroxene and orthopyroxene coexist different calibrations of the two-pyroxenes geothermometer were also used (Wood and Banno 1973; Wells 1977; and Kretz 1981). The ranges of pre-eruptive temperature are 1,100–1,150°C for olivine-rich basaltic andesites, 1,000–1,050°C for basaltic andesites, 900–1,000°C for andesites, and 900–920°C for dacites.

Whole-rock major and trace element chemistry

Sixty-nine whole-rock samples were analysed for major and trace elements; 38 representative analyses are given in Table 4. Figures 6 and 7 contain the full data set, where each analysis was recalculated to 100% on a volatile-free basis and with all Fe as FeO.

The Andahua–Orcopampa and Huambo lavas consist of high-K (1.4–4.4 wt.% K_2O) calc-alkaline lavas, from olivine-rich basaltic andesites to dacites, ranging from 52.1 to 68.1 wt.% SiO_2 (Fig. 6; Peccerillo and Taylor 1976; Le Maître 1989). Andesite is the most abundant and ubiquitous lava type (51 samples), whereas dacites are very scarce (four samples) and limited to the largest volcanic centre (e.g. Puca Mauras in the Orcopampa valley). The three least differentiated olivine-rich basaltic andesites are found in the Huambo area and at Cerro Nicholson. MgO, CaO, FeO_t, Ni, Cr, and V contents show negatively correlated curved trends with SiO_2 abundance (52 to 56 wt.%, Fig. 7). The abundances of most incompatible elements (Rb, Th, U) are positively correlated with SiO_2 content. Al_2O_3, Na_2O, Sr and Ba concentrations display two-step evolution, with increasing trends from 52 to 58 wt.% SiO_2, and decreasing trends for higher SiO_2 contents. Major and trace element evolution is thus broadly consistent with differentiation by fractional crystallization at shallow pressures.

A closer inspection, however, indicates a more complex magmatic evolution. Ba, Pb, Th, U and, to a lesser extent, Na_2O, K_2O, Rb and Sr contents show a high variability in intermediate and evolved lavas, which cannot be attributed to analytical imprecision (see the Analytical method section). Furthermore, data for highly incompatible elements U, Th, Rb and Pb can be interpreted to define two trends for the differentiated lavas of the Puca Mauras composite cone and lava flows located in the Orcopampa field. The curvature in some of the trends on the variation diagrams suggests that if mixing has occurred, the compositional contrast between end-members must have been small. Otherwise, mixing between mafic recharge and evolved dacites would result in linear rather than curved trends.

Thus, a simple crystal fractionation model is not consistent with the observed scatter and, for example, with the evolution of Ba from intermediate to silicic lavas. Decreasing Ba-contents would suggest that biotite and/or sanidine are the dominant fractionating phases from 5 wt.%

Table 4 Major, trace and REE analyses of selected samples from the Andahua–Orcopampa and Huambo volcanic fields and the Cerro Nicholson cone

	vol58	vol60	vol4	vol5	vol6	vol64	vol65	vol66	vol70
Area Location	C.N.	C.N.	H Llajuapampa	H road above C. Marbas	H C. Tururuma	H Marbas Chico lava field	H Marbas Chico lava field	H summit Marbas Grande	H Mojonpampa lava field
Type	OBA	OBA	A	A	OBA	A	A	BA	A
Method	1	2	1	1	2	2	2	1	2
SiO_2	52.46	52.25	57.15	60.33	51.43	58.78	60.65	55.81	58.67
Al_2O_3	16.54	17.18	16.53	16.37	16.71	16.88	16.98	17.20	16.39
Fe_2O_3	9.47	9.29	6.67	5.68	9.03	6.31	5.80	7.51	6.65
MnO	0.12	0.13	0.08	0.07	0.12	0.06	0.06	0.08	0.08
MgO	5.34	5.09	2.84	2.40	7.30	2.77	2.31	3.37	3.03
CaO	8.37	8.19	5.78	5.02	8.72	5.61	4.96	6.40	5.56
Na_2O	3.69	3.54	5.23	4.67	3.37	4.31	4.56	4.80	3.64
K_2O	1.72	1.71	2.85	3.20	1.38	2.87	3.05	2.09	3.10
TiO_2	1.46	1.34	1.26	1.03	1.21	1.03	0.99	1.44	0.96
P_2O_5	0.36	0.38	0.63	0.45	0.29	0.41	0.43	0.58	0.30
LOI	0.37	1.10	0.37	1.05	0.38	0.99	0.24	0.92	1.58
Sum	99.91	100.20	99.39	100.26	99.94	100.02	100.03	100.21	99.96
FeOt	8.52	8.36	6.00	5.11	8.13	5.68	5.22	6.76	5.98
Rb	26	33	49	64	21	63	72	29	81
Sr	864	877	1212	873	594	925	915	1108	693
Ba	653	730	1454	1263	500	1154	1248	1059	907
Zr	155	169	282	269	137	232	258	179	231
Nb	5	6	10	10	5	9	10	7	8
Ni	56	67	17	13	134	22	18	30	28
Cr	<d.l.	91	<d.l.	<d.l.	372	37	28	<d.l.	37
V	<d.l.	241	<d.l.	<d.l.	215	144	131	<d.l.	161
Y	22	20	16	14	16	12	12	13	17
Pb	9	8	<d.l.	<d.l.	3.7	12.8	12.5	9.3	15.1
Th	<d.l.	3.00	<d.l.	4.80	2.21	5.06	5.11	<d.l.	10.59
U	<d.l.	0.62	<d.l.	<d.l.	0.57	0.85	0.89	<d.l.	2.12
La	28.70	31.70	60.28	51.20	19.54	44.83	49.02	40.10	40.87
Ce	62.70	69.75	118.94	100.00	43.04	92.96	104.76	83.00	83.75
Pr	<d.l.	8.50	<d.l.	<d.l.	5.45	11.42	12.89	<d.l.	10.35
Nd	35.50	34.60	50.70	44.00	23.70	42.65	46.61	43.00	38.63
Sm	7.04	6.48	8.45	7.45	4.67	6.78	7.58	7.16	6.46
Eu	1.56	1.87	2.01	1.65	1.42	1.76	1.79	1.71	1.64
Gd	5.80	5.25	5.41	5.12	3.76	4.69	4.60	5.30	4.64
Tb	<d.l.	0.74	<d.l.	<d.l.	0.57	0.59	0.57	<d.l.	0.66
Dy	4.27	3.92	2.84	2.53	2.99	2.81	2.60	3.22	3.33
Ho	<d.l.	0.73	<d.l.	<d.l.	0.61	0.46	0.40	<d.l.	0.61
Er	2.36	1.86	1.28	1.08	1.63	1.14	1.03	1.20	1.64
Tm	<d.l.	0.26	<d.l.	<d.l.	0.21	0.15	0.16	<d.l.	0.20
Yb	1.74	1.89	0.95	0.85	1.41	0.97	0.90	0.92	1.46
Lu	<d.l.	0.26	<d.l.	<d.l.	0.26	0.15	0.12	<d.l.	0.19
$(La/Yb)_N$	15.3	15.6	59.0	56.0	12.8	43.1	50.5	40.6	26.0
Sr/Yb	497	465	1277	1028	420	958	1016	1207	475
Sr/Y	39	43	77	62	37	75	79	83	42

All Fe is given as Fe_2O_3.

Abbreviations for the petrographic types are: *OBA* for olivine-rich basaltic andesites, *BA* for basaltic andesites, *A* for andesites, *D* for dacites. Abbreviations for locations: *CN* Cerro Nicholson, *H* Huambo, *AND* Andahua, *O* Orcopampa. Abbreviations for the method and laboratories where the analyses were performed: (*1*) XRF for major and trace elements and ICP–AES for REE on concentrated fraction by ion-exchange chromatography at Ecole Nationale des Mines de Saint-Etienne, France; (*2*) ICP–MS at CRPG—Nancy, France; and (*3*) ICP–MS and XRF at Geowissenschaftlisches Zentrum of Göttingen Georg-August Universität, Abteilung Geochemie, Germany.

Table 4 (continued)

vol71	vol75	vol77	H99-03	H99-04	H99-05	vol8	vol14	vol15	vol16 A
H Mojon-pampa lava field	H Lava flow Laguna Mucurca	H lava flow from basement	H Marbas Chicas II	H flow below road	H small cone near road	AND lava flow south exit of town	AND Chil-cayoc Chico	AND Jechapita	AND Chilcayoc lava field
BA	BA	A	A	BA	BA	A	A	A	BA
2	2	1	3	3	3	1	1	1	1
54.81	55.25	59.10	59.00	53.7	55.00	58.64	58.12	59.04	54.76
17.51	17.44	16.40	16.50	17.40	16.90	16.51	16.35	16.25	16.47
7.90	7.87	6.52	6.28	8.58	8.07	6.42	6.71	6.21	7.39
0.08	0.08	0.08	0.08	0.11	0.10	0.08	0.08	0.07	0.08
3.83	3.72	3.12	2.78	4.29	4.12	2.76	3.02	2.56	3.39
7.72	7.35	5.41	5.55	7.31	6.88	5.71	5.90	5.34	6.64
4.06	4.14	3.73	4.45	4.36	4.14	4.78	4.95	5.05	4.96
1.92	2.09	3.10	2.87	2.09	2.47	2.24	2.65	2.69	1.92
1.32	1.35	0.99	1.07	1.41	1.43	1.17	1.22	1.16	1.37
0.45	0.46	0.31	0.43	0.49	0.52	0.42	0.52	0.43	0.51
0.39	0.26	0.90				0.28	0.10	0.00	0.22
99.99	100.01	99.66	99.01	99.74	99.63	99.01	99.62	98.80	97.71
7.11	7.08	5.87	5.65	7.72	7.26	5.78	6.04	5.59	6.65
32	37	83	64	29	37	34	42	48	18
1197	1204	650	917	950	938	930	1063	861	114
835	871	940	1228	1130	1130	967	1298	1078	970
154	167	231	232	222	223	180	251	227	194
5	6	8	8	10	8	6	10	9	7
29	28	19	22	43	51	20	20	15	28
43	42	<d.l.	37	69	97	<d.l.	<d.l.	<d.l.	<d.l.
207	205	<d.l.	148	194	190	<d.l.	<d.l.	<d.l.	<d.l.
15	15	17	15	17	15	14	15	15	15
8	9	17	9	67	11	<d.l.	<d.l.	<d.l.	<d.l.
3.95	3.93	8.90	3.29	3.08	3.19	<d.l.	3.20	4.60	3.80
0.75	0.88	<d.l.	1.01	0.82	0.63	<d.l.	<d.l.	<d.l.	<d.l.
33.16	35.90	45.50	37.08	33.18	40.65	31.10	48.37	43.10	34.74
73.93	76.77	89.90	84.08	80.81	92.20	68.20	104.36	89.90	82.02
9.62	10.16	<d.l.	11.35	9.66	10.82	<d.l.	<d.l.	<d.l.	<d.l.
40.86	42.40	42.20	41.69	33.93	42.03	34.60	40.74	41.00	38.99
6.49	7.38	6.98	7.99	6.09	7.34	6.61	7.76	7.63	7.84
1.77	1.91	1.44	1.73	1.56	2.03	1.55	1.71	1.62	1.60
5.13	4.89	5.42	3.93	4.72	5.06	4.49	5.05	5.08	5.37
0.64	0.64	<d.l.	0.53	0.51	0.64	<d.l.	<d.l.	<d.l.	<d.l.
3.11	3.30	3.10	2.50	3.36	2.91	2.44	2.79	2.68	2.80
0.53	0.56	<d.l.	0.54	0.54	0.48	<d.l.	<d.l.	<d.l.	<d.l.
1.48	1.30	1.24	1.27	1.31	1.30	0.97	1.52	1.08	1.25
0.20	0.19	<d.l.	0.13	0.21	0.16	<d.l.	<d.l.	<d.l.	<d.l.
1.20	1.23	0.93	0.85	0.99	0.93	0.74	0.91	0.88	0.84
0.18	0.17	<d.l.	0.13	0.17	0.14	<d.l.	<d.l.	<d.l.	<d.l.
25.7	27.2	45.7	40.6	31.0	40.4	38.8	49.2	45.3	38.4
999	981	702	1082	956	1004	1250	1164	974	1360
79	79	39	61	56	63	680	72	59	76

Table 4 (continued)

vol16 B	vol49	vol54a	vol54b	vol54c	A99-17	A99-18	A99-20	A99-22	A99-27
AND Chilcayoc lava field	AND Chilcayoc Chico	AND basement rock	AND basement rock	AND basement rock	AND Flows W of valley	AND Ticsho	AND Nina-mama	AND Chil-cayoc	AND Chil-cayoc
A	A	A	A	A	A	A	A	A	A
1	2	2	2	2	3	3	3	3	3
56.19	58.33	58.85	58.49	59.08	59.00	58.10	57.60	57.90	56.50
16.4	17.07	16.40	16.66	16.78	16.7	16.60	16.90	16.80	17.20
6.97	6.54	6.63	6.61	6.65	6.19	6.20	6.74	6.59	7.53
0.08	0.07	0.07	0.07	0.07	0.09	0.08	0.09	0.09	0.09
3.14	2.96	2.94	3.07	3.02	2.48	2.59	2.94	2.99	3.41
6.21	5.99	5.41	5.74	5.67	5.54	5.87	6.01	5.90	6.69
5.01	4.69	4.42	4.38	4.47	5.06	4.81	4.94	4.88	4.88
2.17	2.71	2.63	2.58	2.59	2.9	2.73	2.54	2.63	1.97
1.29	1.12	1.14	1.12	1.12	1.17	1.15	1.25	1.19	0.98
0.51	0.49	0.40	0.41	0.39	0.56	0.56	0.56	0.54	0.52
0.00	0.06	1.08	0.85	0.13					
97.98	100.03	99.97	99.98	99.97	99.68	98.68	99.56	99.51	99.77
6.27	5.88	5.97	5.95	5.98	5.57	5.58	6.06	5.93	6.78
28	52	66	60	63	58	44	43	45	25
1076	1076	849	859	861	1116	1272	1149	1115	1196
1014	1243	1045	965	988	1405	1521	1275	1305	991
199	250	234	224	221	255	228	222	233	179
7	10	9	8	8	8	7	7	9	4
23	25	33	35	35	20	19	25	28	33
<d.l.	44	57	58	58	27	30	40	42	52
<d.l.	156	161	159	162	139	137	150	142	183
14	13	14	14	14	14	14	13	13	14
<d.l.	13	13	12	13	13	7	12	12	7
<d.l.	3.75	6.21	5.78	6.16	3.58	3.04	2.01	3.24	1.27
<d.l.	0.73	1.29	1.18	1.24	0.64	0.75	0.61	0.61	0.42
35.90	51.35	43.19	39.38	39.95	49.51	51.96	46.13	47.86	31.49
84.76	109.56	91.45	86.08	86.61	102.85	120.99	89.01	106.40	64.81
<d.l.	12.73	10.80	10.11	10.46	11.68	14.34	11.64	11.88	9.56
36.89	48.29	41.67	39.71	41.21	44.63	46.61	54.62	45.04	39.75
8.51	8.02	7.48	6.96	6.83	7.34	6.88	8.58	7.39	6.53
1.67	2.05	1.76	1.71	1.70	1.89	1.97	2.18	2.05	1.93
4.84	5.14	4.80	4.45	4.69	4.97	5.40	4.39	5.18	3.85
<d.l.	0.66	0.60	0.60	0.61	0.60	0.54	0.71	0.63	0.60
2.54	3.12	3.11	2.86	3.01	2.64	3.03	2.26	2.84	2.22
<d.l.	0.50	0.47	0.48	0.52	0.43	0.51	0.48	0.46	0.48
1.24	1.26	1.19	1.24	1.19	1.09	1.00	1.56	1.23	1.16
<d.l.	0.17	0.16	0.17	0.16	0.13	0.15	0.15	0.16	0.13
0.80	0.99	1.01	1.00	1.03	0.82	0.71	0.89	0.88	0.80
<d.l.	0.13	0.17	0.16	0.16	0.12	0.14	0.11	0.14	0.10
41.5	48.0	39.6	36.7	36.1	56	68	48.2	50.5	36.4
1341	1084	838	863	838	1359	1787	1294	1267	1487
75	80	61	62	63	80	91	88	86	85

Table 4 (continued)

vol22a	vol25	vol29-1	vol32	vol35	vol37	A99-01	A99-10	A99-15
O C. Mauras Sur	O Puca Mauras	O Puca Mauras	O cone NE Puca Mauras	O Challhue Mauras	O Challhue Mauras	O Puca Mauras	O Puca Mauras	O Puca Mauras
A	D	A	BA	A	A	D	A	D
2	2	2	2	1	1	3	3	3
58.23	62.42	59.80	55.68	56.20	59.21	62.4	61.40	64.30
17.19	16.06	16.93	16.96	16.49	17.30	16.1	16.20	15.70
6.51	5.16	5.91	7.24	7.12	6.47	5.16	5.46	4.73
0.07	0.05	0.06	0.08	0.08	0.07	0.07	0.08	0.07
2.13	2.00	2.35	3.05	3.07	2.31	1.97	2.10	1.82
4.90	4.45	5.01	6.66	6.00	5.06	4.35	4.62	4.08
4.74	4.66	4.78	5.14	4.17	4.86	4.41	4.59	4.58
3.17	3.05	2.93	2.61	3.13	2.94	3.35	3.21	3.02
1.07	0.92	1.05	1.25	1.42	1.12	0.94	0.98	0.89
0.54	0.38	0.43	0.62	0.78	0.56	0.37	0.39	0.33
1.51	0.81	0.75	0.79	1.47	0.29			
100.06	99.96	100.000	100.08	99.93	100.19	99.11	99.03	99.51
5.86	4.64	5.32	6.51	6.41	5.82	4.64	4.91	4.26
80	83	78	57	61	75	123	106	88
952	847	972	1342	1288	941	781	845	701
1568	977	1270	1438	1445	1493	1162	1166	826
292	177	226	235	237	278	214	218	150
12	8	9	11	9	11	7	7	7
22	17	18	26	22	15	15	15	17
39	29	25	50	<d.l.	<d.l.	26	25	21
147	119	134	169	<d.l.	<d.l.	109	122	107
14	11	11	15	16	18	12	14	11
8	9	8	7	14	14	16	15	16
5.92	5.67	6.65	4.15	4.80	<d.l.	12.10	10.43	6.32
1.02	2.05	0.98	0.87	<d.l.	<d.l.	1.48	1.36	2.44
63.92	36.80	50.64	62.21	64.40	65.20	42.71	42.65	27.78
125.92	77.80	102.29	125.27	129.00	129.00	92.43	92.87	63.19
14.34	8.80	11.44	14.01	<d.l.	<d.l.	10.25	10.58	7.61
53.81	35.34	42.89	56.40	56.8	56.10	39.24	38.30	30.49
8.09	6.40	6.81	8.88	9.92	8.78	6.16	6.71	5.33
2.06	1.54	1.82	2.12	2.33	2.03	1.55	1.62	1.40
4.65	4.14	4.82	5.47	6.88	6.79	4.38	4.51	3.74
0.66	0.52	0.59	0.73	<d.l.	<d.l.	0.53	0.55	0.47
3.06	2.57	2.57	3.42	3.51	3.40	2.34	2.36	2.20
0.55	0.41	0.40	0.54	<d.l.	<d.l.	0.38	0.39	0.37
1.31	0.96	1.04	1.46	1.51	1.54	0.99	1.00	0.99
0.19	0.15	0.11	0.20	<d.l.	<d.l.	0.13	0.13	0.13
1.15	0.84	0.76	1.16	1.26	1.14	0.77	0.80	0.85
0.17	0.12	0.13	0.18	<d.l.	<d.l.	0.11	0.11	0.11
51.4	40.8	61.9	50.0	47.4	53.1	51.8	49.3	30.4
824	1011	1279	1161	1022	826	1020	1052	827
67	77	89	89	81	52	65	60	64

SiO_2 onwards, but this is not supported by petrographical observations because the main phenocryst phases (olivine, pyroxene, plagioclase) have Ba-partition coefficients significantly less than 1. Alternatively, this decreasing trend may reflect mixing of intermediate andesites with Ba- and Sr-depleted rhyodacitic melts. Such evolved compositions are unknown in the Andahua–Orcopampa and Huambo volcanic province, but have been found in Mio–Pliocene volcanic

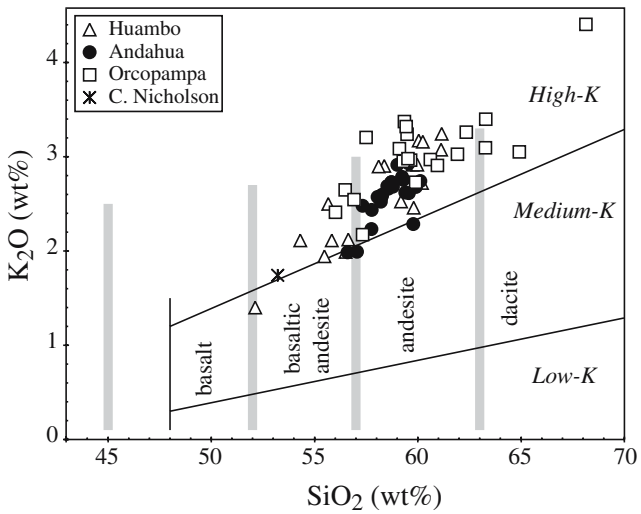

Fig. 6 Classification of calc–alkaline series (Peccerillo and Taylor 1976) modified and simplified by Le Maître (1989) used for the Andahua–Orcopampa and Huambo lavas. The lavas belong to the high-K calc–alkaline field. The oxides contents are recalculated to 100% on a volatile-free basis and with all Fe as FeO

deposits of southern Peru (Vatin-Pérignon et al. 1996). Also, the scatter of data around trends for Rb, Th, and to a lesser extent U and Pb in the Orcopampa intermediate andesites (58 to 64 wt.% SiO_2) indicates magmatic processes other than simple fractional crystallization, and are consistent with additional magma mixing and contamination (see also discussion below on isotopic compositions).

Multi-element patterns of the Andahua–Orcopampa and Huambo lavas normalised to primitive mantle (Fig. 8a) display enrichment in LILE (Cs, Rb, Ba) relative to primitive mantle. Some elements exhibit anomalies relative to their neighbour elements, e.g. Th is depleted relative to Ba and Rb, Pb is enriched relative to Ce, and Nb is depleted relative to K. The low enrichment in Ti, Y and Yb relative to primitive mantle is likely related to occurrence of mineral phases (e.g. garnet or amphibole) that fractionate these compatible elements. The patterns for the Andahua–Orcopampa and Huambo lavas are similar to those observed for CVZ volcanic rocks (Davidson et al. 1991; Stern 2002). Despite a decrease in Sr abundance from 56 wt.% SiO_2 onwards, the lavas do not exhibit any negative Sr-anomaly or Eu-anomaly relative to their neighbours on multi-element patterns normalised to primitive mantle, or on REE patterns normalised to chondrite. The absence of Eu anomalies suggests high fO_2 crystallisation conditions involving Eu preferentially in the 3+ state, or high water pressure, which leads to the reduction of plagioclase crystallization (Sisson and Grove 1993).

REE patterns of the Andahua–Orcopampa and Huambo lavas normalised to chondrite C1 display steep slopes with an enrichment of the LREE (La, Ce) and a depletion in HREE (Fig. 8b) relative to chondrite. $(La/Yb)_N$ displays a rough positive correlation with SiO_2 (Fig. 9). The olivine-rich basaltic andesites, which are considered to be the closest end-member to parental magmas, show the flattest REE patterns, with the lowest LREE and the highest HREE-contents. The REE patterns display enrichment in LREE with increasing degree of differentiation, but a depletion in HREE leading to crossover patterns. Thus there is no overall enrichment in REE from olivine-rich basaltic andesites to dacites as would be typical for simple low-pressure fractionation, suggesting the role of other differentiation processes or decoupled evolutions. The absence of a strong plagioclase signature and these crossover REE patterns, i.e. the depletion in HREE, would be suggestive of garnet fractionation or garnet-bearing, plagioclase-free residues at high pressures.

Oxygen isotope data

Whole-rock O-isotope data for 23 samples from the Andahua–Orcopampa and Huambo Quaternary volcanic province and for four samples of the Cenozoic volcanic and sedimentary formations of the substratum are reported in Table 5. Clinopyroxene and plagioclase separates were also analysed in phenocryst-bearing samples. The Andahua–Orcopampa and Huambo lavas show a considerable range in $\delta^{18}O$ values of whole-rock (7.1–10.0‰) and plagioclase (8.0–12.5‰) and a much narrower range for clinopyroxene (7.5–8.7‰). The olivine-rich basaltic andesites exhibit the lowest $\delta^{18}O$ values except sample vol60, a scoriaceous Cerro Nicholson lava, which exhibits the highest $\delta^{18}O$ value of 10.0‰. The basaltic andesites and andesites show variable O-isotope signatures but no systematic ^{18}O-enrichment with the degree of differentiation as reflected by the silica content (Table 5; Fig. 10).

Assessment of oxygen isotope equilibrium

In young and unaltered volcanic rocks, phenocryst $\delta^{18}O$ values record the distribution of oxygen isotopes between melt and crystals prevailing at the time of crystallisation. Even in such fresh rocks, however, subsolidus oxygen exchange with late-stage external fluids can shift $\delta^{18}O$ values, with plagioclase and the glassy groundmass the constituents most likely to be affected (Gregory and Criss 1986; Davidson and Harmon 1989). Secondary uptake of water through low-temperature hydration (<400°C) should result in a general ^{18}O-enrichment correlated with LOI (as a rough proxy for water contents in the samples). Most of the Andahua–Orcopampa and Huambo samples do not show such correlations for whole-rock data (Fig. 11a), suggesting that low-temperature hydration had little or no

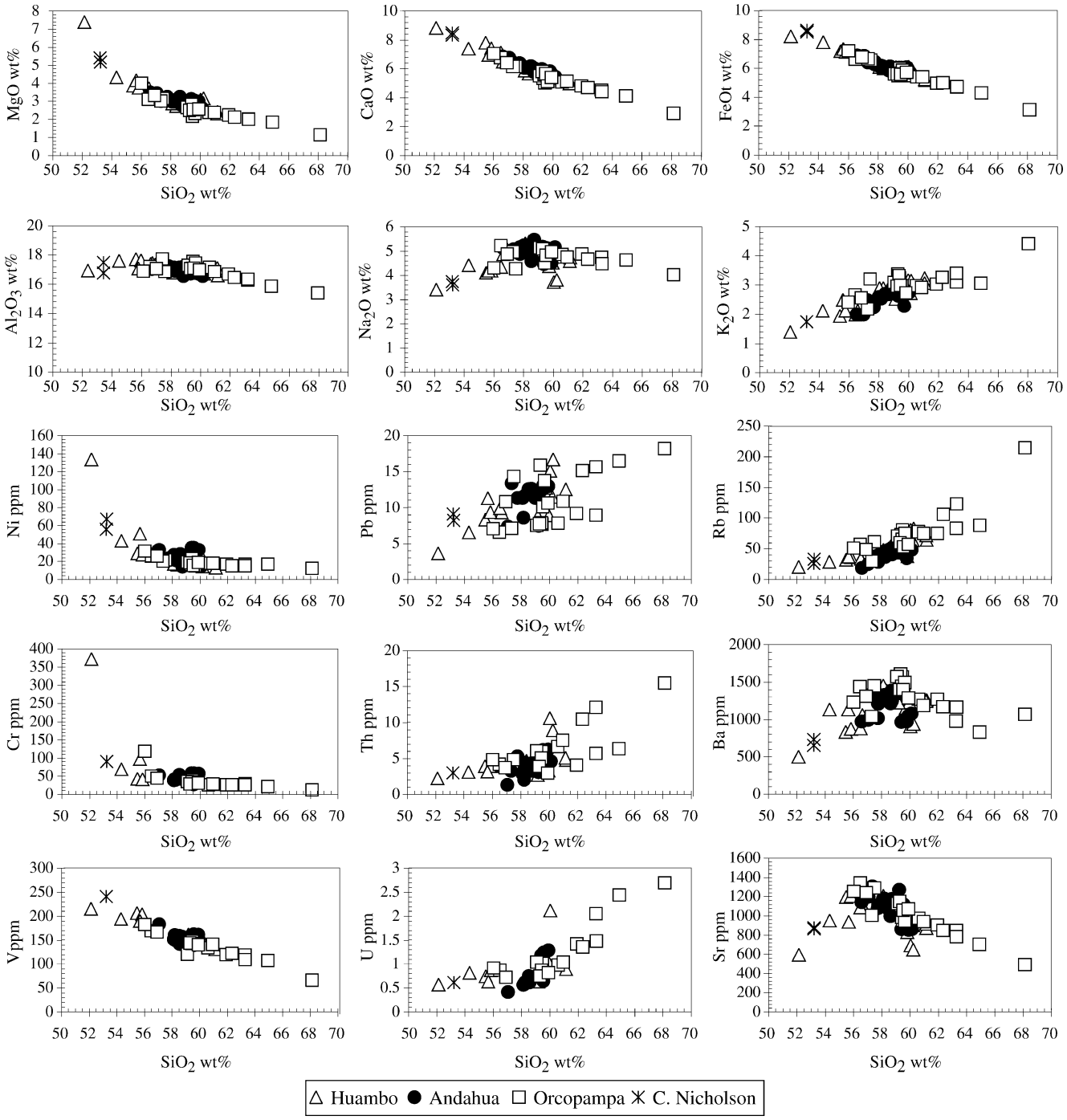

Fig. 7 Harker-type diagrams for major and trace elements compositions of the Andahua–Orcopampa and Huambo lavas. Most of the elements show linear negative or positive trends with SiO_2, but some elements, such as Na_2O, Al_2O_3, and Sr display scattered trends (see text for further discussion). The oxide contents are recalculated to 100% on a volatile free basis and with all Fe as FeO

effect on their O-isotope compositions, except for sample vol60. The oxygen isotopic equilibrium between coexisting minerals at magmatic temperature can also be tested by so-called δ–δ plots (Gregory and Criss 1986). The $\delta^{18}O$ values of plagioclase, which should exchange oxygen relatively rapidly, are reported versus $\delta^{18}O$ values of coexisting clinopyroxene, which should exchange oxygen more slowly, for four samples spanning the whole range of lava compositions from basaltic andesite to dacite (Fig. 11b). The mineral pairs fall within the $\Delta=0.5‰$ and $\Delta=1.6‰$ equilibrium lines, which correspond to the experimental $\Delta_{plag-cpx}$ fractionations (Chiba et al. 1989)

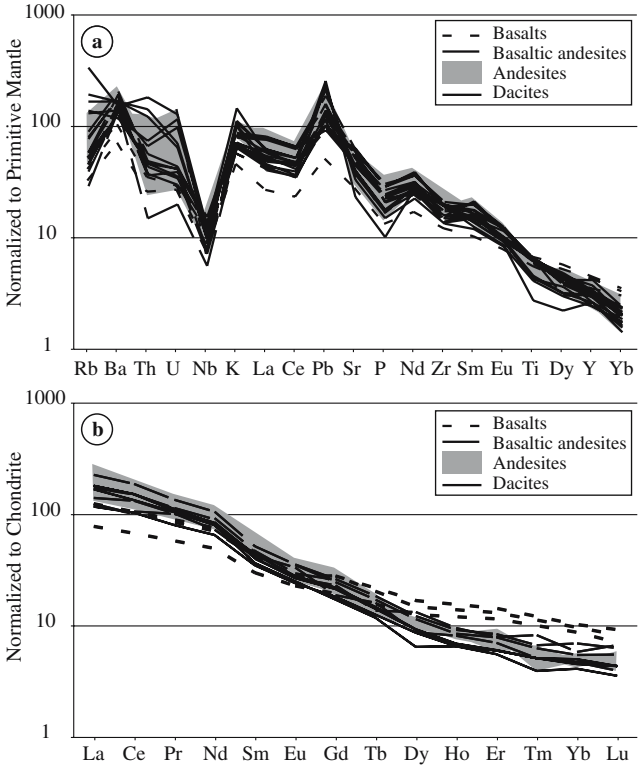

Fig. 8 **a** Multi-element diagrams of the Andahua–Orcopampa and Huambo lavas normalized to primitive mantle (Sun and Mc Donough 1989) showing the typical pattern for lavas related to subduction zones. **b** REE-patterns of the Andahua–Orcopampa and Huambo lavas normalized to chondrite C1 (Sun and Mc Donough 1989)

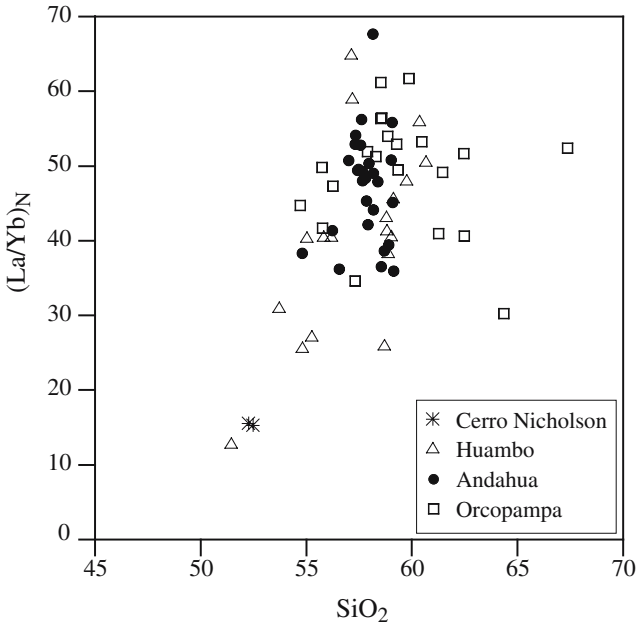

Fig. 9 Diagram of $(La/Yb)_N$ versus SiO_2 for the Andahua–Orcopampa and Huambo lavas showing a positive correlation of the ratio with increasing SiO_2, as well as enrichment in LREE and depletion in HREE of the lavas

for An_{70} at 1200°C and An_{30} at 700°C, respectively. For the other samples, in which only one mineral phase was analysed, $\delta^{18}O$ values are within similar ranges of 7.5–8.5‰ for pyroxene and 8.0–9.8‰ for plagioclase. Thus measured $\delta^{18}O$ are interpreted to reflect magmatic values. Only in the case of sample vol60, with a plagioclase $\delta^{18}O$ value of 12.5‰, is there a suggestion of lower temperature O-reequilibration or a xenocrystic origin for the plagioclase.

Interpretation of oxygen isotope ratios

The most mafic lavas, olivine-rich basaltic andesites, have the lowest $\delta^{18}O$ values of 7.1–7.3‰ but even these are ^{18}O-enriched relative to mantle-derived primitive basaltic magmas of continental subduction zones (Fig. 10), which have an average $\delta^{18}O$ value of 6.2±0.7‰. This is slightly higher than the average value for MORB (5.7±0.2‰), possibly reflecting intramantle subduction zone enrichment processes (Harmon and Hoefs 1995). Consequently a positive shift in the $\delta^{18}O$ values of about 1‰ reflects subsequent assimilation of crustal ^{18}O-rich components at some storage level in the crust by magmas ascending from the mantle wedge. The main problem is to evaluate at which level in the crust this occurs, either by mixing with partial melts from the lowermost crust (MASH zone), or by assimilation of upper crustal components during low-pressure differentiation.

Crystallisation and assimilation

Crystal fractionation is one of several processes including assimilation and/or mixing involved in the differentiation of the Andahua–Orcopampa and Huambo lavas, at least from basaltic andesites to andesites. As noted above, the Andahua–Orcopampa and Huambo lavas have magmatic O-isotope compositions, which allow the investigation of the effect of closed-system crystal fractionation on the $^{18}O/^{16}O$ ratio of differentiating magma. Mineral–magma oxygen isotope fractionations are quite small, generally less than ±1‰, except for magnetite and olivine (Kyser et al. 1981; Kalamarides 1986; Zhao and Zheng 2003). Therefore, if closed system crystal fractionation is the dominant process, the predicted oxygen isotope composition of a derivative dacitic melt would be only 0.6‰ enriched relative to the parent melt (Fig. 10). The observed $\delta^{18}O$ values are systematically higher than predicted values and they do not show a systematic positive correlation with SiO_2. Thus a complex open-system evolution must be inferred. In the absence of low-temperature exchanges, substantial increase in $\delta^{18}O$ values of the order of 1 to 2‰ implies interaction with

Table 5 Sr-, Nd- and O-isotopes ratios for the Andahua–Orcopampa and Huambo minor centres and Cerro Nicholson volcano

Location	Sample n°	Type	SiO_2[b]	LOI	$\delta^{18}O_{WR}$[a]	$\delta^{18}O_{cpx}$[a]	$\delta^{18}O_{plag}$[a]	$^{87}Sr/^{86}Sr$	$^{143}Nd/^{144}Nd$	$^{206}Pb/^{204}Pb$	$^{207}Pb/^{204}Pb$	$^{208}Pb/^{204}Pb$
			Wt.%	Wt. %	(‰ VSMOW)	(‰ VSMOW)	(‰ VSMOW)	(±1σ errorX1000)	(±1σ errorX1000)	(±1σ errorX1000)	(±1σ errorX1000)	(±1σ errorX1000)
Huambo	vol6	OBA	52.1	0.38	+7.26±0.30			0.706693±0.013	0.512396±0.005			
	H99-04	BA	54.3	–				0.706708±0.010	0.512336±0.005	18.298±0.8	15.5577±0.7	38.4891±1.8
	vol71	BA	55.5	0.39	8	7.7	8					
	H99-05	BA	55.7	–				0.706938±0.009	0.512317±0.005	18.315±1.2	15.5679±1.1	35.5455±1.9
	vol75	BA	55.8	0.26	8.3	7.6		0.705909±0.013	0.512509±0.006			
	vol66	BA	56.6	0.92	8.4			0.706113±0.012	0.512503±0.008			
	vol4	A	58.1	0.37	7.8			0.706157±0.011	0.512464±0.006			
	vol70	A	60	1.58	8.9	7.5		0.706592±0.011	0.512382±0.006			
	vol64	A	59.7	0.99	9.4	7.8						
	H99-03	A	60	–				0.706229±0.011		18.576±0.8	15.6012±0.8	38.6428±2.2
	vol5	A	61.2	1.05	8.4	7.7	8					
	vol65	A	61.1	0.24	8.6	8.1		0.706152±0.012	0.512467±0.006			
Andahua	vol16A	BA	56.6	0.22	+7.66±0.02			0.706647±0.011	0.512386±0.006			
	vol16B	A	57.8	0	8.2		9.8	0.706098±0.014	0.512495±0.006			
	A99-27	A	57.1	–				0.706188±0.012	0.512459±0.004	18.586±0.7	15.5732±1.2	38.5227±1.6
	A99-20	A	58.3	–				0.706108±0.010	0.512472±0.005	18.604±1.2	15.5576±1.0	38.5202±2.7
	A99-22	A	58.6	–				0.706120±0.013	0.512464±0.004	18.607±0.7	15.5714±0.6	38.5611±1.8
	A99-18	A	59.3	–				0.706061±0.010	0.512455±0.004	18.629±0.7	15.5833±0.6	38.6207±1.8
	vol14	A	58.8	0.1	8.3		9.4	0.706163±0.013				
	vol49	A	58.7	0.06	8.5							
	vol8	A	59.8	0.28	8.5		9.8					
	A99-17	A	59.6	–				0.706081±0.012	0.512472±0.005			
	vol15	A	60.1	0	7.8	7.9		0.706281±0.012	0.512464±0.006			
Orcopampa	vol32	BA	56.5	0.79	8.6							
	vol35	A	57.5	1.47	+9.32±0.09							
	vol22a	A	59.5	1.51	9.1			0.706085±0.013	0.512485±0.006			
	vol37	A	59.7	0.29	8.7	8.7	9.7	0.706111±0.014	0.512472±0.006			
	vol29-2	A	60.6	0.75	+8.59±0.12			0.706242±0.013	0.512448±0.006			
	A99-10	A	624	–				0.706334±0.011	0.512417±0.006	18.551±0.7	15.5770±0.6	38.5493±1.9
	A99-01	D	63.3	–				0.706371±0.010	0.512415±0.006			
	A99-15	D	64.9	–				0.706281±0.011	0.512426±0.007			
	vol25	D	63.3	0.81	8.2	8.1	9.8	0.706233±0.010				
Cerro	vol58	OBA	53.2	0.37	7.1							
Nicholson	vol60	OBA	53.2	1.1	+10.02±0.05		12.5					
Bedrocks	vol54b	A	59.4	0.85	8.9	7.6	8.2					
	vol54c	A	59.6	0.13	8.6	7.4	8.1					
	vol54a	A	59.9	1.08	8.9	+7.55±0.16	+8.17±0.22	0.706124±0.015	0.512477±0.005			
	vol77	A	60.2	0.9	+8.65±0.28	7.4	9.6					
	vol17	S	98.9	–	+14.45±0.04							

Abbreviations for the petrographic types are: *OBA* for olivine-rich basaltic andesites, *BA* for basaltic andesites, *A* for andesites, *D* for dacites, and *S* for sandstone.

[a] Where replicate analyses were made the average value and ± uncertainty are reported.

[b] SiO_2-contents from analyses recalculated to 100% on a volatile free basis and with all Fe as FeO (as in Fig. 6).

^{18}O-rich crustal components. Progressive assimilation of surrounding crustal materials (AFC) and/or magma mixing with ^{18}O-rich melts can be tested in order to explain the O-isotope signatures of the Andahua–Orcopampa and Huambo lavas. Assimilation–fractional crystallisation is commonly inferred to explain both trace elements and isotopic data of the Peruvian Cenozoic volcanic rocks (James 1982). The effect of continuously assimilating upper crustal rocks with δ^{18}O values ranging from 12 to 22‰ into a crystallizing magma with an initial δ^{18}O= 7.3‰, corresponding to the δ^{18}O value of the more mafic Andahua–Orcopampa and Huambo lavas, is shown in Fig. 10 (AFC, De Paolo 1981). Potential contaminants are the Precambrian Charcani gneisses, i.e. the regional basement in southern Peru with an average δ^{18}O value of 12‰ (James 1982), and two types of sedimentary rocks in the Andahua–Orcopampa and Huambo local basement, sandstones with δ^{18}O values of 14.5‰ and limestones with δ^{18}O values of 21.8‰ (this study). The calculations modelled in Fig. 10 assume constant ratios of crystallizing minerals to assimilated rocks (r=5 and 7) because of heat balance requirements (Table 6). Our calculations of the AFC curves of Fig. 10 also involve an assumption that the effect of the contaminant composition on SiO_2 evolutionary trend is negligible compared to the effects of crystal fractionation because of the small ratio of introduced contaminant to remaining melt at any stage of the process. According to Fig. 10, the Charcani gneisses are plausible contaminants. Furthermore, assimilation of sedimentary rocks may also be inferred on a more local scale to account for δ^{18}O values of up to 9.5‰. However, andesite lavas (58–60 wt.% SiO_2) show the highest δ^{18}O values, whereas lavas with higher SiO_2 content have systematically lower δ^{18}O values (Fig. 10). These features are inconsistent with a simple progressive assimilation of ^{18}O-rich material during differentiation in low-pressure magmatic reservoirs.

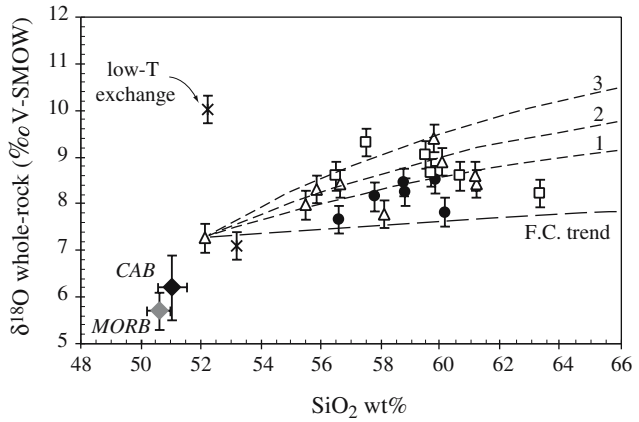

Fig. 10 Plot of whole-rock δ^{18}O values versus silica-content for the Andahua–Orcopampa and Huambo lavas (data in Table 5). *Symbols* for the different areas as in Fig. 6. 2 sigma-error bars for O-isotope data are reported. Average compositions for mid-ocean ridge basalts (*MORB*) and for continental arc basalts (*CAB*) are +5.7±0.2‰ and +6.2±0.7‰, respectively (Harmon and Hoefs 1995). *F.C. trend* represents the δ^{18}O values predicted evolution for magmas differentiating through closed-system fractionation, calculated using a Rayleigh fractionation model assuming that the δ^{18}O value of the olivine-rich basaltic andesite (*vol6*) is the initial magma composition (Table 6): $\delta^{18}O = \left[\left(\delta^{18}O^{initial} + 1000\right)f^{(\alpha-1)}\right] - 1000$ where the isotopic composition of the magma is a function of f, the fraction of remaining melt, and α, the mean isotopic fractionation factor between the crystallising minerals and magma. Curves 1, 2 and 3 are predicted AFC curves in case that differentiating magmas continuously assimilated Charcani gneisses, sandstones or limestones, respectively (see text for explanations). One sample, vol60, is interpreted to have been affected by O-isotope exchanges at low temperature (Fig. 11)

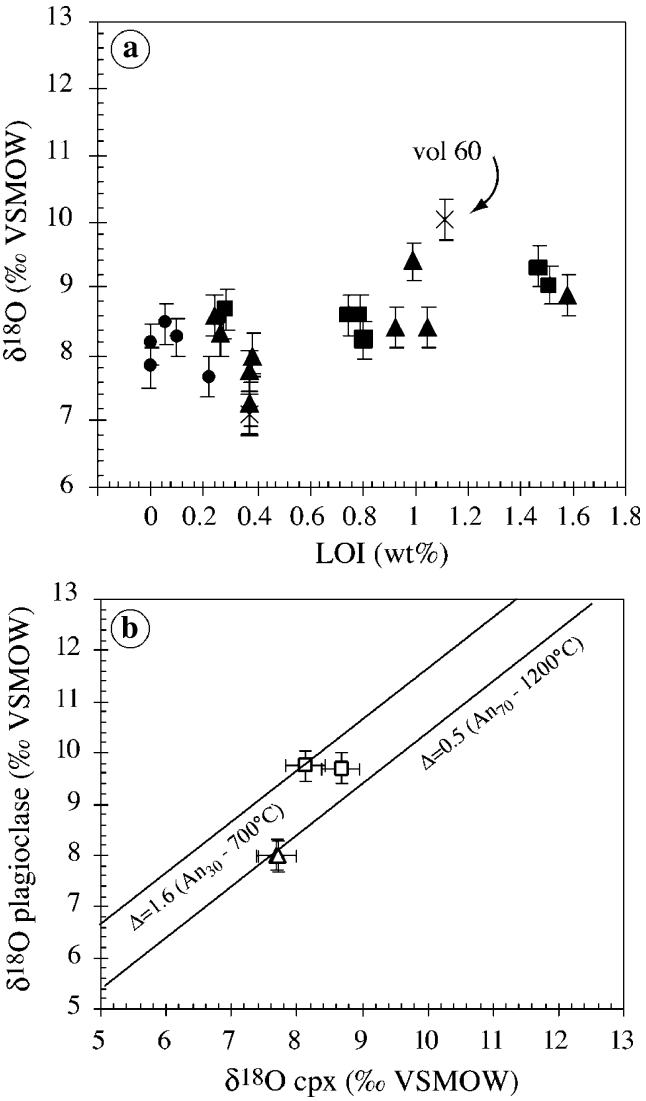

Fig. 11 **a** Plot of whole-rock δ^{18}O values (*filled symbols*) versus *LOI* (=Loss On Ignition). Only O-isotope composition of sample vol60 records the effect of low-temperature re-equilibration. Two sigma-error bars for O-isotope data are shown. **b** Plot of plagioclase δ^{18}O values versus clinopyroxene (*cpx*) δ^{18}O values. Symbols for the different areas as in Fig. 6. Values are consistent with O-isotope equilibrium at magmatic temperatures (see text for explanation)

Table 6 Crystal fractionation model for the Andahua–Orcopampa and Huambo lavas

Phase	Fractionation mineral–magma[a]	Weight percent of extracted mineral[b]	$\delta^{18}O$[c]
1. Olivine-rich basaltic andesite to basaltic andesite			
Olivine-rich basaltic andesite vol6			7.3
Plag (An_{70})	0.15	18.3	
Cpx	−0.35	7.5	
Ol (Fo_{85})	−0.9	7.9	
Mt	−2.05	2.2	
Basaltic andesite vol75: 64 wt.% remaining melt, $\sum r^2=0.01$[d]			7.4
2. Basaltic andesite to andesite			
Basaltic andesite vol75			
Plag (An_{55})	−0.1	22.5	
Cpx	−0.75	6.8	
Ol (Fo_{75})	−1.05	2.4	
Mt	−2.35	3.2	
Andesite vol5: 65 wt% remaining melt, $\sum r^2=0.11$[d]			7.7
3. Andesite to dacite			
Andesite vol5			
Plag (An_{40})	0.05	21.2	
Hornblende	−0.9	11.8	
Mt	−2.6	2.1	
Dacite A99-08: 64 wt% remaining melt, $\sum r^2=0.18$[d]			7.9

[a] Experimental, empirical and theoretically calculated data (Kyser et al. 1981; Kalamarides 1986; Zhao and Zheng 2003)

[b] Data from a numerical simulation of crystal fractionation using least squares regression of the major elements.

[c] Calculated O-isotope model values of magmas derived by crystal fractionation, except for the olivine-rich basaltic andesite value from Table 6

[d] Data for the sum of squares of residuals between calculated and measured compositions

Assimilation in MASH zones

The ^{18}O-enrichment in the more mafic Andahua–Orcopampa and Huambo lavas indicates that even these are affected by assimilation. Partial melting of recently underplated mafic material at the conditions of the CVZ lower crust (MASH zone) will lead to intermediate to high-Si crustal magmas, slightly ^{18}O-enriched compared to the granulitic residue. As granulitic rocks from continental settings have an average $\delta^{18}O$ value of 7.8±1.5‰ (Fowler and Harmon 1990), the O-isotope composition of the olivine-rich basaltic andesite may thus be achieved by mixing of 3:2 to 1:1 ratio of such silicic melt with $\delta^{18}O$= 7.8 to 8.3‰ and mantle-derived magma with $\delta^{18}O$=6.2± 0.7‰ (mean value of continental arc basalts, Harmon and Hoefs 1995). However, this is not consistent with the Sr-, Nd- and Pb-isotopic compositions and the mafic nature of some of the rocks. Contamination probably occurred by partial melting of old crust with evolved Sr-, Pb-isotopic ratios and high $\delta^{18}O$ (see also discussion below on radiogenic isotopic compositions).

Radiogenic isotope data

Twenty-six samples were analysed for Sr- and Nd-radiogenic isotopes and eight were analysed for Pb-isotopes. The results are presented in Table 5. The $^{87}Sr/^{86}Sr$ ratios of the Andahua–Orcopampa and Huambo lavas range from 0.70591 to 0.70694. Three lavas sampled in the Huambo field, the olivine-rich basaltic andesite (vol6) and two basaltic andesites (H99-04 and H99-05) are characterised by the highest $^{87}Sr/^{86}Sr$ values (0.70669, 0.70671, and 0.70694, respectively). The $^{143}Nd/^{144}Nd$ isotope ratios range from 0.512317 to 0.512509 (Table 5). A basaltic andesite located in the Huambo area (vol75) exhibits the lowest $^{87}Sr/^{86}Sr$ ratio and the highest $^{143}Nd/^{144}Nd$ isotope ratio (0.70509 and 0.512509, respectively). The Sr- and Nd-isotope compositions of the Andahua–Orcopampa and Huambo volcanic province are more enriched than other mafic samples analysed by Kay et al. (1994, 1999) from the southern CVZ.

In a graph of $^{143}Nd/^{144}Nd$ versus $^{87}Sr/^{86}Sr$ (Fig. 12a), the Andahua–Orcopampa and Huambo lavas plot in the less-enriched part of the isotopic range for CVZ lavas, and are divided into two groups. The first group is characterised by higher $^{87}Sr/^{86}Sr$ ratios and comprises most of the less differentiated lavas of the three monogenetic fields (vol6, vol16a, vol70, H99-04, H99-05). The second group is formed by the other lavas of Andahua–Orcopampa and Huambo monogenetic fields (basaltic andesites, e.g. vol75, andesites and dacites) and is characterised by higher $^{143}Nd/^{144}Nd$ ratios. The isotopic compositions of the Andahua–Orcopampa and Huambo minor centres define a range of the most primitive lavas encountered in the CVZ. Davidson et al. (1991) studied isotopic compositions of basaltic andesites in the Central Andes, which they have defined as "baseline" compositions. They show a similar but narrower isotopic compositional range to that of the Andahua–Orcopampa and Huambo minor centres. The olivine-rich basaltic andesites and basaltic andesites (the first group) of the Andahua–Orcopampa and Huambo volcanic province are the most primitive lavas within the CVZ. Their Sr-isotopic ratios are still, however, radiogenic, suggesting a strong crustal signature even in these parent "baseline" magmas that may likely feed the composite volcanoes.

The $^{206}Pb/^{204}Pb$ ratios of these lavas range from 18.30 to 18.63, the $^{207}Pb/^{204}Pb$ ratios range from 15.57 to 15.60, and the $^{208}Pb/^{204}Pb$ ratios are from 38.49 to 38.64. These values are in the range of the local metamorphic basement (Barreiro and Clark 1984; Mamani et al. 2004). In a plot of $^{207}Pb/^{204}Pb$ versus $^{206}Pb/^{204}Pb$ (Fig. 12b), the Andahua–Orcopampa and Huambo lavas divide into the same two groups defined by the Sr- and Nd-isotopes. The first group of lavas shows the lowest $^{206}Pb/^{204}Pb$ ratios, and the second group the highest $^{206}Pb/^{204}Pb$ ratios.

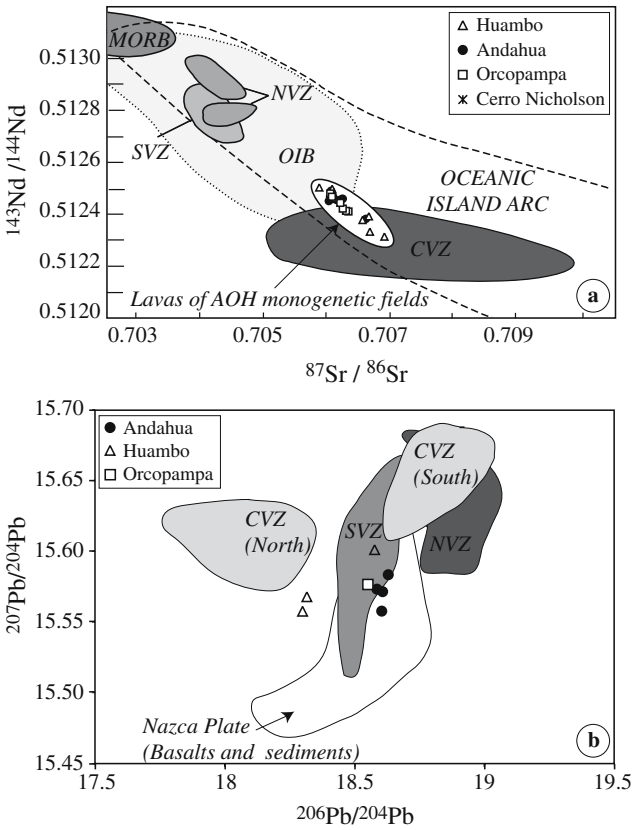

Fig. 12 Radiogenic isotopic compositions of the Andahua–Orcopampa and Huambo lavas. **a** Plot of $^{143}Nd/^{144}Nd$ ratios versus $^{87}Sr/^{86}Sr$ ratios showing the isotopic range for the Andahua–Orcopampa and Huambo lavas within the CVZ. The NVZ, CVZ, OIB fields are drawn after Wilson (1989) **b** Pb-isotopic composition of the Andahua–Orcopampa and Huambo lavas compared to the Andean volcanic fields (*NVZ*, *CVZ*, and *SVZ*; Davidson et al. 1991) and the domain defined by the sediments and basalts of the Nazca Plate

According to Wörner et al. (1992), Aitcheson et al. (1995), and Mamani et al. (2004), there is a clear relationship between the Pb-isotope composition of the metamorphic basement and that of the magmas that ascended through and were contaminated by this continental crust in the Central Andes. Therefore, the Pb-isotope compositions of the Andahua–Orcopampa and Huambo lavas may be interpreted to be dominated by assimilation of the metamorphic basement.

Discussion

Source of Andahua–Orcopampa and Huambo lavas

The source of Andean magmas for the composite volcanoes forming the volcanic zones of the Andes has been extensively investigated (James 1982; Barreiro and Clark 1984; Hildreth and Moorbath 1988; Davidson et al. 1991; Kay et al. 1999; De Silva and Xuming 2000; Gerbe and Thouret 2004) but is still contentious. Because shallow processes have affected the lavas produced by the composite volcanoes, their source is difficult to assess. Magmas erupted from minor, monogenetic, volcanic centres may provide better information concerning the deeper processes and source sites involved in forming Andean magmas (Davidson et al. 1991).

The Pleistocene Andahua–Orcopampa and Huambo volcanic centres display geochemical characteristics similar to those of the composite volcanoes of southern Peru (e.g. Nevado Coropuna and Nevado Sabancaya), which are also high-K calc-alkaline lavas and contain An-rich plagioclase.

The Sr-, Nd-, Pb-, and O-isotope compositions suggest that the Andahua–Orcopampa and Huambo magmas assimilated a crustal component. The assimilation of such material could have occurred at deep levels by mixing of partial melts of the lower crust (MASH zone) with primitive, mantle-derived Andahua–Orcopampa and Huambo magmas.

The most mafic olivine-rich basaltic andesites display the lowest $\delta^{18}O$ values (7.1–7.3‰ SMOW), which are still heavier than those of mantle-derived primitive basaltic magmas of continental subduction zones (6.2±0.7‰, Harmon and Hoefs 1995). These lavas are also characterised by high $^{87}Sr/^{86}Sr$ ratios (~0.7067) and crustal Pb-isotopic compositions, strengthening the argument for a crustal contaminant. Source contamination by subducted sediments has been considered as an alternative to explain crustal $^{18}O/^{16}O$, $^{87}Sr/^{86}Sr$, and $^{206}Pb/^{204}Pb$ ratios of the olivine-rich basaltic andesites and basaltic andesites above subduction zones, e.g. for volcanics of the Mariana island arc (Ito and Stern 1986). Geophysical and sea-bottom imaging work (Thornburg and Kulm 1987) has demonstrated that there are no sediments in the trench off the coast of southern Peru. This is because of an extremely arid climate since about 15 Ma, which mobilised only small amounts of continental sediment; this has been transported to the forearc and captured there, with virtually no sediment entering the trench. Pelagic sediments on the Nazca plate 140 km off the coast of Chile, are mainly calcium carbonate and about 220 m thick (Shipboard Scientific Party 2002). Consequently, subduction of sediments into the mantle source is not a viable process to explain the crustal ^{18}O-, $^{87}Sr/^{86}Sr$ and Pb-isotope signature. Moreover, for a shift from 6.2 to 7.3‰ O-isotope mass balance would require large amounts of sediment in the source (>20%) and this would result in a larger shift in $^{87}Sr/^{86}Sr$ ratios (>0.710).

The Andahua–Orcopampa and Huambo lavas have chemical characteristics (high LREE, high Sr contents, low Y contents, low HREE, and high $(La/Yb)_N$ ratios >30; Table 4) that are similar to those of adakitic-type magmas. Indeed, their high $(La/Yb)_N$ and Sr/Y ratios plot close to or within the adakite field (Fig. 13a, b). It is unlikely, however, that Andahua–Orcopampa and Huambo lavas

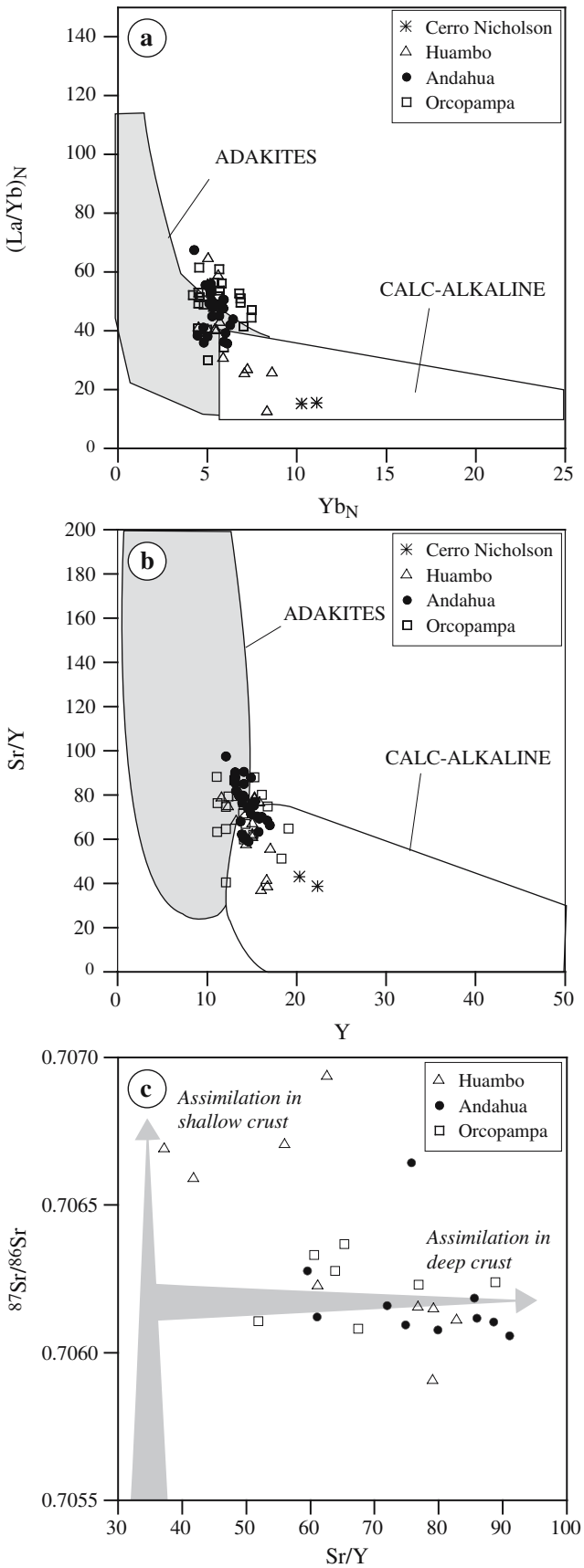

Fig. 13 Adakitic signature of the Andahua–Orcopampa and Huambo lavas. **a** Plot of the $(La/Yb)_N$ versus Yb_N showing that the Andahua–Orcopampa and Huambo lavas plot within and adjacent to the adakite field. **b** Plot of Sr/Y versus Y showing that the Andahua–Orcopampa and Huambo lavas plot across the boundary between the adakite and calc–alkaline fields. **c** Plot of $^{87}Sr/^{86}Sr$ versus Sr/Y showing that the Andahua–Orcopampa and Huambo lavas have a low Sr/Y ratio for high $^{87}Sr/^{86}Sr$ ratios while their Sr/Y decreases for lower $^{87}Sr/^{86}Sr$ isotopic ratios. This strengthens the hypothesis that crustal melts generated with a garnet-bearing residue are involved in forming magmas below the southern Peruvian Andes

are real adakites. Adakites are defined as products of melting of young and hot oceanic lithosphere during subduction (Defant and Drummond 1990). Several authors (Defant 2002; Kay 2002) have pointed out that this type of process is totally unrealistic in the subduction setting of the Central Andes (old and "cold" oceanic crust, 60–70 km thick continental crust) and that another set of processes may lead to the same chemical characteristics.

In the Northern Volcanic zone of the Andes, where the slab is younger, Garrison and Davidson (2003) have also demonstrated that adakitic-type geochemical signatures, such as high Sr/Y (>40), is not specific of slab-melting and may be produced by melting of any metamorphosed basalt. Thus the adakitic signature is not indicative of slab-melting but may related to a large variety of arc magmatic processes.

Geophysical data indicate that the Peruvian continental crust is abnormally thick (60–70 km; Barazangi and Isacks 1976; Isacks 1988; Beck and Zandt 2002), and that partial removal of the mantle lithosphere occurs, allowing hot asthenospheric material to fill the gap between the crust and the subducting plate. This hot asthenospheric material may enhance heating and partial melting of the lower crust, following delamination (Whitman et al. 1992, 1996; Kay and Kay 1993; Kay et al. 1994; Babeyko et al. 2002). The lower crustal materials tend to have mainly a mafic composition (Yuan et al. 2002). If such partial melts are mixed with mantle-derived basaltic arc magmas in a high-pressure MASH (melting, assimilation, storage and homogenisation (Hildreth and Moorbath 1988)) zone, then magmas with adakitic signatures will be produced. The lower crust is likely to be old, with elevated Sr- and crustal Pb-isotopic ratios (Fig. 12) and high $\delta^{18}O$ values. Thus, assimilation by mantle-derived arc magmas of partial melts generated at high pressure with a garnet-bearing granulitic residue (>15 kbar) would have generated the isotopic and geochemical signatures of the Andahua–Orcopampa and Huambo magmas (Figs. 13c and 14).

Evolution of the Andahua–Orcopampa and Huambo magmas

The Andahua–Orcopampa and Huambo magmas were already contaminated by a lower crustal component in a high-pressure MASH zone before ascent and storage at upper levels of the crust. Judging from the Cr-spinel compositional range, the olivine-rich basaltic andesites did not suffer prolonged storage prior to their eruption. They were thus prevented from extended low-pressure interactions with the upper crust.

The Andahua-Orcopampa and Huambo monogenetic fields occupy a specific tectonic setting. They are situated in the vicinity of regional scale fault zones, including the NW–SE-trending Huanca and Ichupampa faults. Four major fault groups were identified within the Andahua–Orcopampa and Huambo volcanic province. Many of these faults are inherited from previous major tectonic phases of Andean orogeny and may have their roots quite deep in the lithosphere (Fig. 2b). The current north–south extensional regime of southern Peru has reactivated the N120–N130 trending and N80-trending faults, which could create deep pathways for ascending magmas (Huaman et al. 1993; Mering et al. 1996). The relatively fast-ascending and small volumes of Andahua–Orcopampa and Huambo magmas moving through these fractures are more difficult to contaminate at shallow crustal levels than are magmas in long-lived magmas chambers, such as those of composite volcanoes.

Although there are some indications of open-system fractional crystallisation and local contamination for some minor centres (scattering of major and trace elements, Fig. 7, and $\delta^{18}O$ trend versus SiO_2, Fig. 10), most of the cone magmas did not experience significant shallow level crustal contamination. The anti-correlation between Sr/Y and Sr-isotopes (Fig. 13c) indicates assimilation at high pressure, i.e. in the garnet stability field. Such a correlation is not observed for the composite volcanoes of the CVZ, because shallow level crustal assimilation overprinted it. The Andahua–Orcopampa and Huambo monogenetic centres do exhibit this anti-correlation, indicating that they were not influenced by strong upper crustal contamination. Moreover, the absence of an Eu-anomaly even in relatively evolved magmas, which would be indicative of extensive low-P plagioclase fractionation, suggests that these magmas ascended relatively fast from deeper MASH zones without much fractionation and/or assimilation at shallow crustal levels. Accordingly, deep "mashed"-baseline magmas (sensu Hildreth and Moorbath 1988) can be quite variable in major element composition (mafic to silicic andesite) while their isotopic signatures are relatively similar. We infer that the Andahua–Orcopampa and Huambo magmas represent base-line magmas in southern Peru.

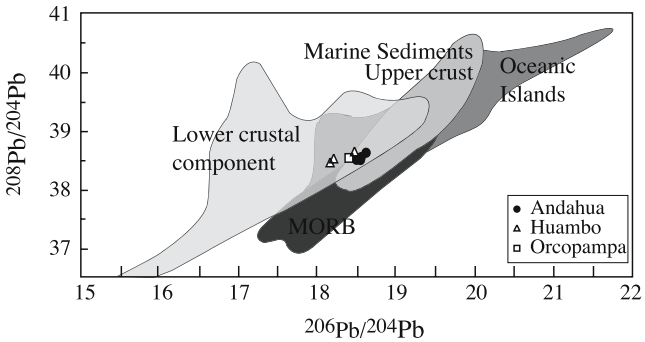

Fig. 14 Pb-isotopic composition of the Andahua–Orcopampa and Huambo lavas (diagram modified after White 2005) showing the effects of assimilation of the lower crust on mantle-derived basaltic arc magmas

Conclusion

Our study of the Andahua–Orcopampa and Huambo monogenetic fields of the CVZ indicates the importance of such minor centres for (1) identifying the most primitive magmas in southern Peru, and (2) defining the compositional range of magmas that probably ascended from deep crustal levels through regional crustal faults. These magmas represent the direct products of deep crustal MASH zones that provide the input into large composite volcanoes in the Central Andes.

In detail, the Sr-, Nd-, Pb-, and O-isotope compositions of the most mafic Andahua–Orcopampa and Huambo lavas reveal that these magmas suffered assimilation by lower-crustal partial melts with granulitic garnet-bearing residues in a high pressure MASH zone. Possible contaminants are the Charcani gneisses and the local Andahua–Orcopampa and Huambo basements. Shallow level crustal assimilation is limited for the Andahua–Orcopampa and Huambo magmas.

Acknowledgements The authors are grateful to M. Veschambre for assistance on the electron microprobe, and C. Perrache and C. Bosq, G. Hartman and K. Simon for invaluable help in REE and radiogenic isotopes analyses. We also thank our Peruvian colleagues and PhD students of IGP (Instituto Geofisico del Peru, Lima) for their support in the field. We gratefully acknowledge the constructive comments of Richard Price, Suzanne Kay and the associate editor, James White, which greatly improved this manuscript. Funding and logistical support for this project were provided by IRD (Institut de Recherche pour le Développement, Lima, Peru), by LMV (Laboratoire Magmas et Volcans UMR 6524 CNRS, Clermont, France), by CRV (ex-Coordination de la Recherche Volcanologique, Clermont) and by IGP (Lima, Peru). Financial support to GW was provided by DFG project Wo362/18.

Appendix

Appendix A Morphometric parameters (based on Wood 1980) measured on topographic maps (scale 1:50,000) and aerial photographs (scale 1:30,000) for the Andahua, Orcopampa, and Huambo volcanic minor centres

Field name	Edifice name	D_b (m)	D_{cr} (m)	H (m)	S (°)	^{14}C age	Time/Generations
Orcopampa	Cerro Mauras	750	175	100	19.2		Late Pleistocene
	Pabellon Mauras	675	75	110	20.1		Late Pleistocene
	Chalhue Mauras	1,050	350	200	29.7		Late Pleistocene
	Yana Mauras	1,600	600	250	26.5	2,810–2,970±50 year BP	Early/mid. Holocene
	Cerro Mauras II	1,000	350	160	26.2		Early/mid. Holocene
	Puca Mauras	1,000	250	400	46.8		Late Holocene
	Santa Rosa	625	225	50	15.0		Late Pleistocene
	Puca Mauras pq.	687	127	166	30.6		Late Pleistocene
Andahua	Cerro Tichso	700	224	117	26.3	4,060±50 year BP	Early/mid. Holocene
	Cerro Yanamauras	625	250	115	31.5		Late Holocene
	Cerro la Cruz	462	150	105	33.9		Late Holocene
	Cerro Cochapampa	675	325	50	16.0		Late Pleistocene
	Jenchana	650	75	110	20.9		Historical
	Chilcayoc pq. I	300	125	50	29.0		Historical
	Chilcayoc pq. II	300	25	50	33.0		Historical
	Jechapita	500	80	125	30.8		Historical
	Chilcayoc Grande	675	188	156	32.6	A.D. 1451 to 1523	Historical
Huambo	Cerro Marbas Grande	1,100	375	200	28.8		Late Holocene
	Marbas	1,075	225	190	24.1		Late Holocene
	Marbas Chico I	750	160	166	29.4		Early/mid. Holocene
	Marbas Chico II	875	80	200	26.7		Early/mid. Holocene

References

Aitcheson SJ, Forrest AH (1994) Quantification of crustal contamination in open magmatic systems. J Petrol 35:461–488

Aitcheson SJ, Harmon RS, Moorbath S, Schneider A, Soler P, Soria-Escalante E, Steele G, Swainbank I, Wörner G (1995) Pb isotopes define basement domains of the Altiplano, Central Andes. Geology 23:555–558

Allmendiger RW, Eremchuck JE, Sosa-Gomez J, Ojeda J, Francis PW (1989) The Pasto–Ventura pull-apart and southward collapse of the southern Puna plateau. J Latin Am Earth Sci 2:111–130

Antayhua Y, Tavera H, Bernal I (2001) Analisis de la actividad sismica en la region del volcán Sabancaya (Arequipa). Bol Soc Geol Perú 92:78–79

Babeyko AY, Sobolev SV, Trumbull RB, Oncken O, Lavier LL (2002) Numerical models of crustal scale convection and partial melting beneath the Altiplano–Puna Plateau. Earth Planet Sci Lett 199:373–388

Bacon CR, Hirschmann MM (1988) Mg/Mn partitioning as a test for equilibrium between coexisting Fe–Ti oxides. Amer Mineral 73:57–61

Barazangi W, Isacks BL (1976) Spatial distribution of earthquakes and subduction of the Nazca plate beneath South America. Geology 4:686–692

Barreiro BA, Clark AH (1984) Lead isotopic evidence for evolutionary changes in magma-crust interaction, Central Andes, southern Peru. Earth Planet Sci Lett 69:30–42

Baumont D, Paul A, Zandt G, Beck SL (2001) Inversion of Pn travel times for lateral variations of Moho geometry beneath the Central Andes and comparison with the receiver functions. Geophys Res Lett 28:1663–1666

Beck SL, Zandt G (2002) The nature of the orogenic crust in the Central Andes. J Geophys Res 107:1–16

Beck S, Zandt G, Myers SL, Wallace T, Silver P, Drake LP (1996) Crustal thickness variations in the Central Andes. Geology 24:407–410

Cahill TA, Isacks BL (1992) Seismicity and shape of the subducted Nazca plate. J Geophys Res 97:17503–17529

Caldas J (1993) Geologia de los cuadrangulos de Huambo y Orcopampa. Bull Inst Geol Minar Metal Lima 46:1–62

Chiba H, Chacko T, Clayton RN, Goldsmith JR (1989) Oxygen isotope fractionations involving diopside, forsterite, magnetite and calcite; application to geothermometry. Geochim Cosmochim Acta 53:2985–2995

Churikova T, Dorendorf F, Wörner G (2001) Sources and fluids in the mantle wedge below Kamchatka, evidence from across-arc geochemical variation. J Petrol 42:1567–1593

Clayton RN, Mayeda TK (1963) The use of bromine pentafluoride in the extraction of oxygen from oxides and silicates for isotopic analyses. Geochim Cosmochim Acta 27:43–52

Colton HS (1967) The basaltic cinder cones and lava flows of the San Francisco Mountain volcanic field, Arizona. Museum of Northern Arizona Bulletin:10 (revised), Flagstaff, pp 1–50

Coplen TK (1993) Normalization of oxygen and hydrogen isotope data. Chem Geol 72:293–297

Davidson JP, Harmon RS (1989) Oxygen isotope constraints on the petrogenesis of volcanic arc magmas from Martinique, Lesser Antilles. Earth Planet Sci Lett 95:255–270

Davidson JP, de Silva SL (1995) Late Cenozoic magmatism of the Bolivian Altiplano. Contrib Mineral Petrol 119:387–408

Davidson JP, Harmon RS, Wörner G (1991) The source of the Central Andean Magmas; Some considerations. In: Harmon RS, Rapela CW (eds) Andean magmatism and its tectonic setting. Geol Soc Am, Special Paper 265:233–243

Defant MJ (2002) Forum. EOS 83(23):256–257

Defant MJ, Drummond MS (1990) Derivation of some modern island arc magmas by melting of young subducted lithosphere. Nature 347:662–665

De Paolo DJ (1981) Trace elements and isotopic effects of combined wallrock assimilation and fractional crystallization. Earth Planet Sci Lett 53:189–202

Deruelle B (1982) Petrology of Plio-Quaternary volcanism of the south central and meridional Andes. J Volcanol Geotherm Res 14:77–124

De Silva SL, Xuming L (2000) Trace element character of minor centres from southern Peru: insight into source relationships beneath the Central Volcanic Zone of the Andes. In: Abstract of State of the Arc 2000 (IAVCEI) Processes and Time Scales in the Genesis and Evolution of Arc Magmas, Ruapehu New Zealand, pp 41–44

Dick HJB, Bullen T (1984) Chromian spinel as a petrogenetic indicator in abyssal and alpine-type peridotites and spatially associated lavas. Contrib Mineral Petrol 86:54–76

Fisk MR, Bence AE (1980) Experimental crystallization of chrome spinel in FAMOUS basalt 527-1-1. Earth Planet Sci Lett 48:111–123

Fowler MB, Harmon RS (1990) The oxygen isotope composition of lower crustal granulite xenoliths. In: Vielzeuf D, Vidal Ph (eds) Granulites and crustal evolution. Kluwer, Dordrecht, pp 493–506

Garrison JM, Davidson JP (2003) Dubious case for slab melting in the Northern volcanic zone of the Andes. Geology 6:565–568

Gerbault M, Martinod J, Hérail G (2005) Possible orogeny-parallel lower crustal flow and thickening in the Central Andes. Tectonophysics 399:59–72

Gerbe MC, Thouret JC (2004) Role of magma mixing in the petrogenesis of tephra erupted during the 1990–98 explosive activity of Nevado Sabancaya, southern Peru. Bull Volcanol 66:541–561

Giese P, Scheuber E, Schilling F, Schmitz M, Wigger P (1999) Crustal thickening processes in the Central Andes and the different natures of the MOHO discontinuity. In: Reutter KJ (ed) Central Andean deformation. J S Amer Earth Sci 12:201–220

Gregory-Wodzicki KM (2000) Uplift history of the Central and Northern Andes: A review. Geol Soc Amer Bull 112:1091–1105

Gregory R, Criss RE (1986) Isotopic exchange in open and closed systems. In: Valley JW, Taylor HP Jr, O Neil JR (ed) Stable isotopes in high temperature geological processes. Rev Miner 16:91–127

Harmon RS, Hoefs J (1984) Oxygen isotope ratios in Late Cenozoic Andean Volcanics. In: Harmon RS, Barreiro BA (eds) Andean Magmatism: Chemical and isotopic constraints, Shiva, London, pp 9–20

Harmon RS, Hoefs J (1995) Oxygen isotope heterogeneity of the mantle deduced from global ^{18}O systematics of basalts from different geotectonic settings. Contrib Mineral Petrol 120:95–114

Harmon RS, Barreiro BA, Moorbath S, Hoefs J, Francis PW, Thorpe RS, Deruelle B, McHugh J, Viglino JA (1984) Regional O-, Sr-, and Pb-isotope relationships in late Cenozoic calc–alkaline lavas of the Andean Cordillera. J. Geol Soc 141:803–822

Hildreth W, Moorbath S (1988) Crustal contributions to arc magmatism in the Andes of Central Chile. Contrib Mineral Petrol 98:455–489

Huaman D, Chorowicz J, Deffontaines B, Guillande R, Rudaut JP (1993) Cadre structurale et risques géologiques étudiés à l'aide de l'imagerie spatiale : la région du Colca (Andes du Sud Pérou). Bull Soc Géol Fr 164:807–818

Irvine TN (1967) Chromian spinel as a petrogenetic indicator Part 2, Petrologic applications. Can J Earth Sci 2:648–671

Isacks BL (1988) Uplift of the central Andean plateau and bending of the Bolivian orocline. J Geophys Res 93:3211–3231

Ito E, Stern RJ (1986) Oxygen- and strontium-isotopic investigations of subduction zone volcanism; the case of the Volcano Arc and the Marianas island arc. Earth Planet Sci Lett 76:312–320

James DE (1971) Plate tectonics and structure of the Andean orogenic belt. EOS, Trans Amer Geophys Union 52(4):351

James DE (1982) A combined O, Sr, Nd, and Pb isotopic and trace element study of crustal contamination in Central Andes lavas, I Local geochemical variations. Earth Planet Sci Lett 57:47–62

Jurewicz AJG, Watson EB (1988) Cations in olivine, Part 1: Calcium partitioning and calcium–magnesium distribution between olivine and co-existing melts, with petrologic applications. Contrib Mineral Petrol 99:176–185

Kalamarides RI (1986) High temperature oxygen isotope fractionation among phases of the Kiglapait intrusion, Labrador, Canada. Chem Geol 58:303–310

Kaneoka CJ, Guevara C (1984) K–Ar determinations of late tertiary and quaternary Andean volcanic rocks, in Southern Peru. Geochem J 18:233–239

Kay SM (2002) Andean adakites from slab melting, crustal thickening, and fore-arc subduction erosion, 5th International Symposium of Andean Geodynamics, pp 405–408

Kay RW, Kay SM (1993) Delamination and delamination magmatism. Tectonophysics 219:177–189

Kay SM, Maksaev V, Moscoso R, Mpodozis C, Nasi C (1987) Probing the evolving Andean lithosphere: Mid-late Tertiary magmatism in Chile (29°–30° 30′S) over the modern zone of subhorizontal subduction. J Geophys Res 92:6173–6189

Kay SM, Coira B, Viramonte J (1994) Young mafic back-arc volcanic rocks as indicators of continental lithospheric delamination beneath the Argentine Puna plateau, Central Andes. J Geophys Res 99:24323–24336

Kay SM, Mpodozis C, Coira B (1999) Neogene magmatism, tectonics, and mineral deposits of the central Andes (22 to 33° S). In: Skinner BJ (ed) Geology and Ore deposits of the Central Andes. Soc Economic Geol Spec Publ 7:27–59

Kretz R (1981) Transfer exchange equilibria in a portion of the pyroxene quadrilateral as deduced from natural and experimental data. Geochim Cosmochim Acta 46:411–421

Kyser TK, O'Neil JR, Carmichael SE (1981) Oxygen isotope thermometry of basic lavas and mantle nodules. Contrib Mineral Petrol 77:11–23

Lamb S (2000) Active deformation in the Bolivian Andes, South America. J Geophys Res 106:25627–25653

Leake BE, Woolley AR, Arps CES, Birch WD, Gilbert MC, Grice JD, Hawthorne FC, Kato A, Kisch HJ, Krivovichev VG, Linthout K, Laird J, Mandarino JA, Maresch WV, Nickel EH, Rock NMS, Schumacher JC, Smith DC, Stephenson NCN, Ungaretti L, Whittaker EJW, Youzhi G (1997) Nomenclature of amphiboles: report of the subcommittee on Amphiboles of the International Mineralogical Association, Commission on New Minerals Names. Am Miner 82:1019–1037

Leeman WP (1978) Distribution of Mg^{2+} between olivine and silicate melt, and its implications regarding melt structure. Geochim Cosmochim Acta 42:789–800

Le Maitre RW (ed) (1989) A classification of igneous rocks and glossary of terms: recommendations of the International Union of Geological Sciences Subcommission on the Systematics of Igneous Rocks. Blackwell, Oxford, pp 193

Mamani M, Wörner G, Ruprecht P, Hartmann G, Simon K (2004) Sources of Central Andean Magmatism in time and space: implications from geochemical data from Quaternary to Miocene volcanism in S Peru and N Chile. International Association of

Volcanology and Chemistry of the Earth's Interior, Pucón Chile, pp 14–19 Nov
Mercier JL, Sebrier M, Lavenu A, Cabrera J, Bellier O, Dumont JF, Machare J (1992) Changes in the tectonic regime above a subduction zone of Andean type; the Andes of Peru and Bolivia during the Pliocene–Pleistocene. J Geophys Res 97:11945–11982
Mering C, Huaman D, Chorowicz J, Deffontaines B, Guillande R (1996) New data on the geodynamics of Southern Peru from computerized analysis of SPOT and SAR ERS-1 images. Tectonophysics 259:153–169
Morimoto N (1988) Nomenclatures of pyroxenes. Can Mineral 27:143–156
Norabuena E, Leffler-Grivin L, Mao A, Dixon T, Stein S, Selwyn-Sacks I, Ocola L, Ellis M (1998) Space geodetic observations of Nazca–South America convergence across the Central Andes. Science 279:358–362
Norabuena EO, Dixon TH, Stein S, Harrison CGA (1999) Decelerating Nazca–South America and Nazca–Pacific plate motions. Geophys Res Lett 26:3405–3408
Peccerillo A, Taylor SR (1976) Geochemistry of the Eocene calc–alkaline volcanic rocks from the Kastamonu area, northern Turkey. Contrib Mineral Petrol 58:63–81
Pin C, Santos Zalduegui JF (1997) Sequential separation of light rare-earth elements, thorium and uranium by miniaturized extraction chromatography: application to isotopic analyses of silicate rocks. Anal Chim Acta 339:79–89
Pin C, Briot D, Bassin C, Poitrasson F (1994) Concomitant separation of strontium and samarium–neodynium for isotopic analysis in silicate samples, based on specific extraction chromatography. Anal Chim Acta 298:209–217
Roeder PL, Emslie RF (1970) Olivine-liquid equilibrium. Contrib Mineral Petrol 29:275–289
Ruprecht P, Wörner G, Kronz A (2006) Variable regimes in magma systems documented in plagioclase zoning patterns: El Misti stratovolcano and Andagua monogenetic cones (S Peru) (submitted to Contrib Mineral Petrol)
Sébrier M, Soler P (1991) Tectonics and magmatism in the Peruvian Andes from late Oligocene time to Present. Bull Geol Soc Amer Special Paper 265:259–277
Shipboard Scientific Party (2002). Leg 202 Preliminary Report. ODP Prelim Report, 102 [Online] http://www-odp.tamu.edu/publications/prelim/202_prel/202PREL.PDF
Sisson TW, Grove TL (1993) Experimental investigations of the role of H_2O in calc–alkaline differentiation and subduction zone magmatism. Contrib Mineral Petrol 113:143–166
Somoza R (1998) Updated Nazca (Farallon)–South America relative motions during the last 40 My; implications for mountain building in the Central Andean region. J S Amer Sci 11:211–215
Spencer KJ, Lindsley DH (1981) A solution model for co-existing iron–titanium oxides. Amer Mineral 11–12:1189–1201
Stern RJ (2002) Subduction zones. Rev Geophys 40:31–38
Sun SS, Mc Donough WF (1989) Chemical and isotopic systematics of oceanic basalts: implications for mantle composition and processes In: Saunders AD, Norry MJ (eds) Magmatism in the Ocean Basins. Geol Soc London Spec Publ 42:313–345
Tassara A (2005) Interaction between the Nazca and South American plates and formation of the Altiplano–Puna plateau: review of a flexural analysis along the Andean margin (15°–34°S). Tectonophysics 399:39–57
Thornburg TM, Kulm LD (1987) Sedimentation in the Chile Trench; depositional morphologies, lithofacies, and stratigraphy. Geol Soc Amer Bull 98:33–52
Thorpe RS, Francis PW, O'Callaghan L (1984) Relatives roles of source composition, fractional crystallization and crustal contamination in the petrogenesis of Andean volcanic rocks. Phil Trans R Soc Lond 310:675–692
Thouret JC, Juvigné E, Gourgaud A, Boivin P, Dávila J (2002) Reconstruction of the AD 1600 Huaynaputina eruption based on the correlation of geologic evidence with early Spanish chronicles. J Volcanol Geotherm Res 115:529–570
Todt W, Cliff RA, Hanser A, Hoffman AW (1984) ^{202}Pb–^{205}Pb spike for Pb analysis. Terra Cognita 4:209
Vatin-Pérignon N, Poupeau G, Oliver RA, Lavenu A, Labrin E, Keller F, Bellot-Gurlet L (1996) Trace and rare-earth element characteristics of acidic tuffs from southern Peru and northern Bolivia and a fission-track age for the sillar of Arequipa. J S Amer Earth Sci 9:91–109
Vennemann TW, Smith HS (1990) The rate and temperature of reaction of ClF_3 with silicate minerals, and their relevance to oxygen isotope analysis. Chem Geol, Isot Geosci Sect 86:83–88
Venturelli G, Fragipane M, Weibel M, Antiga D (1978) Trace element distribution in the Cenozoic lavas of Nevado Coropuna and Andagua Valley, Central Andes of Southern Peru. Bull Volcanol 41:213–228
Vicente JC, Sequeiros F, Valdivia MA, Zavala J (1979) The Cincha–Lluta Overthrust; elements of a major Andean discontinuity in northwestern Arequipa. Bol Soc Geol Peru 61:67–99
Victor P, Oncken O, Glodny J (2004) Uplift of the western Altiplano plateau: Evidence from the Precordillera between 20° and 21°S (northern Chile). Tectonics 23:1–24
Wells PRA (1977) Pyroxene thermometry in simple and complex systems. Contrib Mineral Petrol 62:129–140
White WM (2005) Geochemistry. An online text book. http://www.geo.cornell.edu/geology/classes/geo455/Chapters.HTML
Whitman D, Isacks BL, Chatelain JL, Chiu JM, Perez A (1992) Attenuation of high-frequency seismic waves beneath the central Andean plateau. J Geophys Res 97:19929–19947
Whitman D, Isacks LB, Kay SM (1996) Lithospheric structure and along-strike segmentation of the Central Andean Plateau; seismic Q, magmatism, flexure, topography and tectonics. In: Dewey JF and Lamb SH (ed) Geodynamic of the Andes. Tectonophysics 259:29–40
Wilson M (1989) Igneous petrogenesis. Chapman & Hall, London
Wood CA (1980) Morphometric analysis of cinder cone degradation. J Volcanol Geotherm Res 8:137–160
Wood BJ, Banno S (1973) Garnet–orthopyroxene and orthopyroxene–clinopyroxene relationships in simple and complex systems. Contrib Mineral Petrol 42:109–124
Wörner G, Moorbath S, Harmon RS (1992) Andean Cenozoic volcanics reflect basement isotopic domains. Geology 20:1103–1106
Wörner G, Uhlig D, Kohler I, Seyfried MH (2002) Evolution of the West Andean Escarpment at 18°S (N Chile) during the last 25 Ma: uplift, erosion and collapse through time. Tectonophysics 345:183–198
Yuan X, Sobolev SV, Kind R (2002) Moho topography in the Central Andes and its geodynamic implications. Earth Planet Sci Lett 199:389–402
Zandt G, Velasco AA, Beck S (1994) Central Andean lithosphere structure from slant stacking for teleseismic depth-phase precursors. EOS, Trans Amer Geophys Union 75(44):69
Zhao Z, Zheng Y (2003) Calculation of oxygen isotope fractionation in magmatic rocks. Chem Geol 193:59–80